SISALv3: a global speleothem stable isotope and trace element database

Journal Article

Author(s):
Kaushal, Nikita; Lechleitner, Franziska A.; Wilhelm, Micah; Azennoud, Khalil; Bühler, Janica C.; Braun, Kerstin; Brahim, Yassine Ait; Baker, Andy; Burstyn, Yuval; Comas-Bru, Laia; Fohlmeister, Jens; Goldsmith, Yonaton; Harrison, Sandy P.; Hatvani, István G.; Rehfeld, Kira; Ritzau, Magdalena; Skiba, Vanessa; Stoll, Heather; Szűcs, József G.; Tanos, Péter; Endres, Laura; et al.

Publication date:
2024

Permanent link:
https://doi.org/10.3929/ethz-b-000671803

Originally published in:
Earth System Science Data 16(4), https://doi.org/10.5194/essd-16-1933-2024

Earth Syst. Sci. Data, 16, 1933–1963, 2024
https://doi.org/10.5194/essd-16-1933-2024

Open Access Earth System Science Data

SISALv3: a global speleothem stable isotope and trace element database

Nikita Kaushal[1,a,★], Franziska A. Lechleitner[2,★], Micah Wilhelm[3], Khalil Azennoud[4], Janica C. Bühler[5], Kerstin Braun[7], Yassine Ait Brahim[4], Andy Baker[8], Yuval Burstyn[9,10], Laia Comas-Bru[11], Jens Fohlmeister[12], Yonaton Goldsmith[13], Sandy P. Harrison[14], István G. Hatvani[15,16], Kira Rehfeld[5,6], Magdalena Ritzau[5], Vanessa Skiba[17,18], Heather M. Stoll[19], József G. Szűcs[20], Péter Tanos[20], Pauline C. Treble[8,21], Vitor Azevedo[22], Jonathan L. Baker[23,24], Andrea Borsato[25], Sakonvan Chawchai[26], Andrea Columbu[27], Laura Endres[19], Jun Hu[28], Zoltán Kern[15,16], Alena Kimbrough[29], Koray Koç[30,31], Monika Markowska[32,33], Belen Martrat[34], Syed Masood Ahmad[35], Carole Nehme[36], Valdir Felipe Novello[5], Carlos Pérez-Mejías[23], Jiaoyang Ruan[37,38], Natasha Sekhon[39,40], Nitesh Sinha[37,38], Carol V. Tadros[8,21], Benjamin H. Tiger[41,42], Sophie Warken[43,44], Annabel Wolf[45], Haiwei Zhang[23], and SISAL Working Group members[✚]

[1]Exeter College, University of Oxford, Oxford, OX1 3DP, UK
[2]Department of Chemistry, Biochemistry and Pharmaceutical Sciences, and Oeschger Centre for Climate Change Research, University of Bern, 3012 Bern, Switzerland
[3]Forest Dynamics, Swiss Federal Institute for Forest, Snow and Landscape Research WSL, 8903 Birmensdorf, Switzerland
[4]International Water Research Institute, Mohammed VI Polytechnic University, Lot 660 Hay Moulay Rachid, Ben Guerir, 43150, Morocco
[5]Department of Geoscience, Geo- und Umweltforschungszentrum (GUZ), 72076 Tübingen, Germany
[6]Department of Physics, Geo- und Umweltforschungszentrum (GUZ), 72076 Tübingen, Germany
[7]Institute of Human Origins, Arizona State University, Tempe, AZ 85287, USA
[8]School of Biological, Earth and Environmental Sciences, UNSW Sydney, Sydney, NSW 2052, Australia
[9]UC Davis Institute for the Environment, University of California Davis, Davis, CA 95616, USA
[10]UC Davis Earth and Planetary Sciences, University of California Davis, Davis, CA 95616, USA
[11]independent researcher, 08041 Barcelona, Spain
[12]Environmental Radioactivity, Federal Office for Radiation Protection, 10318 Berlin, Germany
[13]The Fredy & Nadine Herrmann Institute of Earth Sciences, The Hebrew University, Edmond J. Safra Campus – Givat Ram, Jerusalem, 9190401, Israel
[14]Department of Geography and Environmental Science, University of Reading, Reading, RG6 6AH, UK
[15]Institute for Geological and Geochemical Research, HUN-REN Research Centre for Astronomy and Earth Sciences, 1112 Budapest, Hungary
[16]HUN-REN, CSFK, MTA Centre of Excellence, 1121 Budapest, Hungary
[17]Potsdam Institute for Climate Impact Research (PIK), 14473 Potsdam, Germany
[18]Alfred Wegener Institute (AWI), Helmholtz Centre for Polar and Marine Research, 14473 Potsdam, Germany
[19]Department of Earth Sciences, ETH Zurich, 8092 Zurich, Switzerland
[20]Department of Geology, Institute of Geography and Earth Sciences, ELTE Eötvös Loránd University, 1117 Budapest, Hungary
[21]ANSTO – Australia's Nuclear Science and Technology Organisation, Lucas Heights, NSW 2234, Australia
[22]Department of Geology, Trinity College Dublin, Dublin 2, Ireland
[23]Institute of Global Environmental Change, Xi'an Jiaotong University, Xi'an, Shaanxi, 710049, China
[24]Institute of Geology, Innsbruck University, Innrain 52, 6020 Innsbruck, Austria
[25]School of Environmental and Life Sciences, The University of Newcastle, NSW 2308, Australia

Published by Copernicus Publications.

[26]Department of Geology, Faculty of Science, Chulalongkorn University, Bangkok, 10330, Thailand
[27]Department of Earth Sciences, University of Pisa, Via Santa Maria 53, 56126 Pisa, Italy
[28]College of Ocean and Earth Sciences, Xiamen University, Xiamen, Fujian, 361102, China
[29]School of Earth, Atmospheric and Life Sciences, University of Wollongong, Wollongong, NSW 2522, Australia
[30]Department of Geological Engineering, Akdeniz University, 07100 Antalya, Türkiye
[31]Quaternary Geology, Department of Environmental Sciences, University of Basel, 4056 Basel, Switzerland
[32]Department of Climate Geochemistry, Max Planck Institute for Chemistry, 55128 Mainz, Germany
[33]Department of Geography and Environmental Sciences, Northumbria University, Newcastle upon Tyne, NE1 8ST, UK
[34]Department of Environmental Chemistry, Institute of Environmental Assessment and Water Research (IDAEA-CSIC), 08034 Barcelona, Spain
[35]Inter-University Accelerator Centre, New Delhi, 110067, India
[36]UMR IDEES 6266, CNRS, University of Rouen Normandy, 1 Rue Thomas Becket, 76130 Mont-Saint-Aignan, France
[37]Center for Climate Physics, Institute for Basic Science, Busan, 46241, Republic of Korea
[38]IBS Center for Climate Physics, Pusan National University, Busan, 46241, Republic of Korea
[39]Department of Earth, Environmental and Planetary Science, Brown University, Providence, RI 02908, USA
[40]Institute at Brown for Environment and Society, Brown University, Providence, RI 02908, USA
[41]Department of Earth, Atmospheric and Planetary Sciences, Massachusetts Institute of Technology, Cambridge, MA 02139, USA
[42]Department of Geology and Geophysics, Woods Hole Oceanographic Institution, Woods Hole, MA 02543, USA
[43]Institute of Earth Sciences, Ruprecht Karl University Heidelberg, 69120 Heidelberg, Germany
[44]Institute of Environmental Physics, Ruprecht Karl University Heidelberg, 69120 Heidelberg, Germany
[45]Department of Earth System Science, University of California Irvine, Croul Hall, Irvine, CA 92697-3100, USA
[a]now at: American Museum of Natural History, NY 10024, USA
✚A full list of authors appears at the end of the paper.
★These authors contributed equally to this work.

Correspondence: Nikita Kaushal (nikitageologist@gmail.com), Franziska A. Lechleitner (franziska.lechleitner@unibe.ch), and Micah Wilhelm (micah.wilhelm@wsl.ch)

Received: 5 September 2023 – Discussion started: 13 September 2023
Revised: 9 March 2024 – Accepted: 11 March 2024 – Published: 26 April 2024

Abstract. Palaeoclimate information on multiple climate variables at different spatiotemporal scales is becoming increasingly important to understand environmental and societal responses to climate change. A lack of high-quality reconstructions of past hydroclimate has recently been identified as a critical research gap. Speleothems, with their precise chronologies, widespread distribution, and ability to record changes in local to regional hydroclimate variability, are an ideal source of such information. Here, we present a new version of the Speleothem Isotopes Synthesis and AnaLysis database (SISALv3), which has been expanded to include trace element ratios and Sr isotopes as additional, hydroclimate-sensitive geochemical proxies. The oxygen and carbon isotope data included in previous versions of the database have been substantially expanded. SISALv3 contains speleothem data from 365 sites from across the globe, including 95 Mg/Ca, 85 Sr/Ca, 52 Ba/Ca, 25 U/Ca, 29 P/Ca, and 14 Sr-isotope records. The database also has increased spatiotemporal coverage for stable oxygen (892) and carbon (620) isotope records compared with SISALv2 (which consists of 673 and 430 stable oxygen and carbon records, respectively). Additional meta information has been added to improve the machine-readability and filtering of data. Standardized chronologies are included for all new entities along with the originally published chronologies. Thus, the SISALv3 database constitutes a unique resource of speleothem palaeoclimate information that allows regional to global palaeoclimate analyses based on multiple geochemical proxies, permitting more robust interpretations of past hydroclimate and comparisons with isotope-enabled climate models and other Earth sys-

tem and hydrological models. The database can be accessed at https://doi.org/10.5287/ora-2nanwp4rk (Kaushal et al., 2024).

1 Introduction

Speleothems, secondary cave carbonate precipitates, are a rich palaeoenvironmental archive of geochemical data (Wong and Breecker, 2015). Due to their widespread distribution (Comas-Bru et al., 2020) and their precise chronologies (Henderson, 2006), they can provide palaeoclimate data at a seasonal (Baldini et al., 2021) to multi-annual resolution spanning millennial and longer timescales (Cheng et al., 2016; Stoll et al., 2022).

The Speleothem Isotopes Synthesis and AnaLysis working group (SISAL WG) is an international effort to synthesize speleothem data under the umbrella of the Past Global Changes (PAGES) project (Comas-Bru et al., 2017; Comas-Bru and Harrison, 2019). The SISAL WG aims to answer critical open questions in palaeoclimate science with a focus on regional to global trends and event synchronization. To address these questions, the SISAL WG has been developing standardized and quality-checked databases. The first three versions of the database (SISALv1, SISALv1b, and SISALv2) provided the palaeoclimate community with a growing resource of speleothem geochemical data (Atsawawaranunt et al., 2018; Comas-Bru et al., 2020, 2019), specifically oxygen (δ^{18}O) and carbon (δ^{13}C) isotope records, and age-model ensembles, along with an online tool – the SISAL webApp – to increase accessibility to the SISAL database (Hatvani et al., 2024). The SISAL database versions have been exploited (i) to better understand the drivers of speleothem environmental proxies and improve their interpretations (Baker et al., 2019, 2021; Fohlmeister et al., 2020; Treble et al., 2022; Skiba and Fohlmeister, 2023); (ii) to provide a resource for the interpretation of speleothem records at a regional level, identifying key gaps and future work (Kaushal et al., 2018; Lechleitner et al., 2018; Braun et al., 2019b; Burstyn et al., 2019; Deininger et al., 2019; Kern et al., 2019; Oster et al., 2019; Zhang et al., 2019; Lorrey et al., 2020); and (iii) to understand the mechanisms of past climate change, including through comparison with isotope-enabled climate models (Comas-Bru et al., 2019; Parker et al., 2021b; Bühler et al., 2022; Parker and Harrison, 2022; Parker et al., 2021a) and other modelling approaches (Skiba et al., 2023).

The new SISALv3 database provides an increased dataset of oxygen and carbon isotope data, interpreted as records of hydroclimate and vegetation dynamics/bioproductivity (Wong and Breecker, 2015), and has been significantly expanded to include data on Sr, Mg, Ba, and U, which are typically tracers for hydrological processes in the karst and cave (Fairchild et al., 2000; Johnson et al., 2006; Fairchild and Treble, 2009; Wassenburg et al., 2016), and data on P, which is recognized as a tracer for surface bioproductivity (Treble et al., 2003; Borsato et al., 2007; McDonough et al., 2022) (Table 1). Also included are data on Sr isotopes, as these are an important proxy for hydroclimatic processes and may provide information on local hydrology and soil source, production, and/or erosion (e.g. (Li et al., 2005; Ünal-İmer et al., 2016; Wortham et al., 2017; Weber et al., 2018; Ward et al., 2019; Utida et al., 2020). Ratios of Sr/Ca, Mg/Ca, Ba/Ca, and U/Ca, coupled with δ^{13}C information, are sensitive to water–rock interactions and residence time (Fairchild et al., 2000; Johnson et al., 2006). An important mechanism that drives variability in these multiple proxies in quantifiable ways is the process of prior calcite/carbonate precipitation (PCP), through which carbonate precipitated along flow paths in the karst and on the cave roof, leading to an altered element concentration in cave drip waters from which the speleothem ultimately precipitates (Fairchild et al., 2000; Day and Henderson, 2013). An increase in PCP usually occurs in times of drought that facilitate increased water–rock residence times and degassing in the karst (Fairchild et al., 2000). The strength of these proxies is that they provide robust climatic and environmental information via a multi-proxy approach that will need to be tailored for different karst and climatic settings (Table 1). The SISAL WG is currently working on projects with the new additional proxies to explore and gain more detailed insights. We provide examples of proxy interpretations with linked references, but we must emphasize that this list is not exhaustive, the interpretations are timescale dependent, and (in most cases) multi-proxy approaches are necessary (Table 1). Thus, the SISALv3 database augmented with trace element proxies provides a multi-proxy dataset that can be used for long-term drought reconstructions in the past as well as to better understand the forcings, mechanisms, and periodicities of such events. In addition to the new geochemical data, extensive metadata including information on parameters such as vegetation and karst type as well as entity (i.e. speleothem dataset) images are provided to aid robust interpretations.

The SISALv3 database will allow the systematic and global analysis of stable isotope and trace element variability and will elucidate how trace element data can be used to strengthen climatic interpretations from speleothem oxygen (δ^{18}O) and carbon (δ^{13}C) records. The database can be accessed at https://doi.org/10.5287/ora-2nanwp4rk (Kaushal et al., 2024).

Table 1. Summary of speleothem geochemical proxies included in SISALv3, examples of their possible interpretations, and relevant references.

Proxy	Potential drivers	Selected relevant references
$\delta^{18}O$	Semi-quantitative temperature reconstruction dependent on the combined effect of temperature dependency of meteoric precipitation $\delta^{18}O$ and in-cave temperature on carbonate $\delta^{18}O$	Dorale et al. (1998); Mangini et al. (2005); Moseley et al. (2015); Koltai et al. (2017); Wendt et al. (2021); Luetscher et al. (2021); Wolf et al. (2024); Wainer et al. (2011)
	Change in source water composition, e.g. as tracers of ice sheet meltwater during deglaciations	Stoll et al. (2022); Badertscher et al. (2011); Frumkin et al. (1999); Meckler et al. (2012)
	Change in moisture transport trajectory or change in moisture source (sometimes linked to seasonality)	Lachniet et al. (2014); Cheng et al. (2016); Luetscher et al. (2021); Frumkin et al. (1999)
	Change in seasonality of precipitation, e.g. increase in winter rain versus summer rain in different climate states	Cheng et al. (2009b); Baldini et al. (2019); Cheng et al. (2019); Wang et al. (2001)
	Precipitation amount at the cave site and upstream rainout	Bar-Matthews et al. (2003); Hu et al. (2008); Cheng et al. (2016); Columbu et al. (2019); Cheng et al. (2013)
	Large-scale circulation and supra-regional climate, e.g. the Indian summer monsoon	Cheng et al. (2016); Kathayat et al. (2016)
	Recharge processes and karst flow paths	Ayalon et al. (1998); Baker et al. (2019); Treble et al. (2022)
$\delta^{13}C$	Semi-quantitative temperature reconstruction linked to changes in vegetation and soil respiration (requires additional proxies, e.g. Mg/Ca)	Genty et al. (2003, 2006); Lechleitner et al. (2021); Stoll et al. (2022, 2023)
	Vegetation density variability, e.g. low-vegetation-density zones versus high-vegetation-density zones	Fohlmeister et al. (2020)
	Metabolic pathway, e.g. C_3 versus C_4 pathway	Baker et al. (1997)
	Hydroclimate through the prior calcite precipitation mechanism and/or drip rate changes (requires additional proxies, e.g. Mg/Ca)	Johnson et al. (2006); Owen et al. (2016); Carolin et al. (2019b); Fairchild et al. (2000)
Mg/Ca	Hydroclimate through the prior calcite precipitation mechanism and/or drip rate changes, potential for semi-quantitative precipitation reconstruction (requires additional proxies, e.g. $\delta^{13}C$, Sr/Ca, and Ba/Ca, and/or cave monitoring data)	Johnson et al. (2006); Owen et al. (2016); Carolin et al. (2019b); Fairchild et al. (2000); Warken et al. (2018)
	Hydroclimate through dust activity and marine aerosol input (requires additional proxies, e.g. Na/Ca, Sr/Ca, and Ba/Ca, and/or cave monitoring data)	Faraji et al. (2023); Carolin et al. (2019b)
	Hydroclimate through water residence time in soil and karst	Roberts et al. (1998); Treble et al. (2003); Tremaine and Froelich (2013)
Sr/Ca	Hydroclimate through the prior calcite precipitation mechanism and/or drip rate changes (requires additional proxies, e.g. $\delta^{13}C$, Mg/Ca, and Ba/Ca, and/or cave monitoring data)	Johnson et al. (2006); Owen et al. (2016); Carolin et al. (2019b); Fairchild et al. (2000)
	Aeolian transport (increased confidence in interpretation with $^{87}Sr/^{86}Sr$ data)	Goede et al. (1998)
Ba/Ca	Hydroclimate through the prior calcite precipitation mechanism and/or drip rate changes (requires additional proxies e.g. $\delta^{13}C$, Mg/Ca and Sr/Ca, and/or cave monitoring data)	Johnson et al. (2006)
	Growth rate	Treble et al. (2003)
	Soil mineral weathering	Riechelmann et al. (2020); Rutlidge et al. (2014)
U/Ca	Hydroclimate through the prior aragonite precipitation mechanism and/or drip rate changes (requires additional proxies, e.g. $\delta^{13}C$, Mg/Ca, Ba/Ca, and Sr/Ca, and/or cave monitoring data)	Jamieson et al. (2016)
	Enhanced infiltration via complexes (e.g. uranyl phosphate) (requires additional proxies, e.g. P/Ca)	Treble et al. (2003)
P/Ca	Biomass cycling including wildfire; enhanced infiltration via complexes	Huang et al. (2001); Treble et al. (2003); Borsato et al. (2007); McDonough et al. (2022)
Sr isotopes	Hydroclimate through proportional source changes	Verheyden et al. (2000); Utida et al. (2020)
	Aeolian activity	Li et al. (2005)

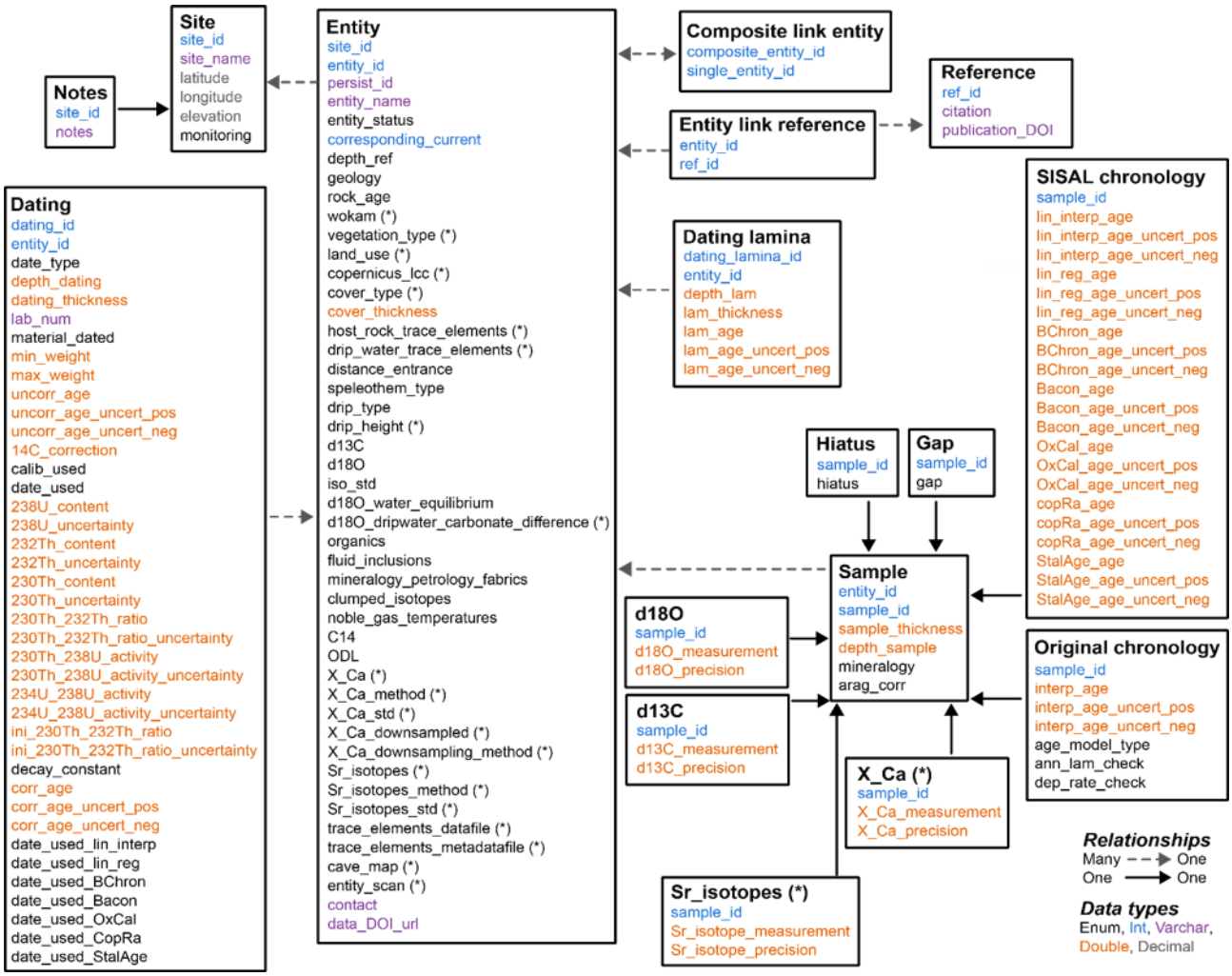

Figure 1. Structure of the SISALv3 database. Fields and tables marked with (*) refer to new information added in SISALv3; see Table 2 for details. The colours refer to the format of that field: Enum, Int, Varchar, Double, or Decimal. More information on the list of predefined menus can be found in the Supplement (Table S1). For trace element records, a series of identical tables was generated (labelled *X*_Ca, where *X* stands for the specific element: Mg, Sr, Ba, U, or P).

2 Data and methods

2.1 New data formatting and processing

All trace elements are reported normalized as ratios with respect to Ca (X/Ca, where X stands for the individual elements) in units of millimoles per mole. In the following paper, "trace element" refers to the normalized ratio to Ca. A standardized conversion sheet is used to facilitate conversions from grams to moles (available in the repository). Sr-isotope data are reported as $^{87}Sr/^{86}Sr$ values. For internal consistency and to facilitate future intercomparison and synthesis studies, the measurement method and reference materials used as well as the measurement precision are also reported for both trace elements and Sr isotopes.

Mechanisms relevant to hydroclimate interpretations from speleothems are based on a multi-proxy approach of stable isotopes and one or more trace element ratios. Therefore, the SISALv3 database structure allows for trace element measurements to be added at the depths of the stable isotope measurements on a given entity. However, between 35 % and 86 % of the records (depending on the element) were measured using in situ techniques, such as laser ablation inductively coupled plasma mass spectrometry (LA-ICP-MS), and these datasets are typically generated at a higher resolution (10–100 µm) than the stable isotope records (Jochum et al., 2012). These data have been downsampled to the resolution of the stable isotope data for the same speleothem. Downsampling was performed by computing averages (and standard deviations) of the trace element measurements for the corresponding stable isotope sampling depths. This implicitly assumes that the same or a (depth-equivalent) parallel sampling track was used for trace elements and stable iso-

Table 2. Changes made to the Site, Entity, and stable isotope tables compared with SISALv2.

Action	Field label	Description	Format	Constraints
Changes made to the Site table				
Field removed	*geology*			
Field removed	*rock_age*			
Changes made to the Entity table				
Field added	*persist_id*	Persistent, unique identifier for each speleothem	Text	
Field added	*geology*	Information on the geology	Text	Selection from predefined list
Field added	*rock_age*	Information on the bedrock age	Text	Selection from predefined list
Field added	*wokam*	Information on the type of carbonate/evaporite rock from the WoKAM database	Text	Added by SISAL Steering Committee (SC) at the database level
Field added	*vegetation_type*	Information on the vegetation cover	Text	Selection from predefined list
Field added	*land_use*	Information on the land use (publication/data contributors)	Text	Selection from predefined list
Field added	*copernicus_lcc*	Information on the land cover from the Copernicus LLC dataset	Text	Added by SISAL SC at the database level
Field added	*cover_type*	Information on the land cover (publication/data contributors)	Text	Selection from predefined list
Field added	*host_rock_trace_elements*	Indication of whether trace element data from the host rock have been measured	Text	Selection from predefined list
Field added	*drip_water_trace_elements*	Indication of whether trace element data from the drip water have been measured	Text	Selection from predefined list
Field added	*drip_height*	Information on the drip height (in m)	Numeric	Free to fill
Field added	*iso_std*	Information on the reference material used for oxygen and carbon isotope measurements	Text	Selection from predefined list
Field added	*d18O_dripwater_carbonate_difference*	Information on the difference between drip water and carbonate oxygen isotope values	Numeric	Free to fill
Field removed	*trace_elements*			
Field added	*Sr_Ca*	Indication of whether Sr/Ca data have been measured	Text	Selection from predefined list
Field added	*Sr_Ca_method*	Information on the measurement method for Sr/Ca	Text	Selection from predefined list
Field added	*Sr_Ca_std*	Information on the reference material used for Sr/Ca measurements	Text	Selection from predefined list
Field added	*Sr_Ca_downsampled*	Information on whether Sr/Ca data had to be downsampled	Text	Selection from predefined list
Field added	*Sr_Ca_downsampling_method*	Information on the downsampling method for Sr/Ca, if applicable	Text	Selection from predefined list
Field added	*Mg_Ca_method*	Information on the measurement method for Mg/Ca	Text	Selection from predefined list
Field added	*Mg_Ca_std*	Information on the reference material used for Mg/Ca measurements	Text	Selection from predefined list
Field added	*Mg_Ca_downsampled*	Information on whether Mg/Ca data had to be downsampled	Text	Selection from predefined list
Field added	*Mg_Ca_downsampling_method*	Information on the downsampling method for Mg/Ca, if applicable	Text	Selection from predefined list
Field added	*Ba_Ca*	Indication of whether Ba/Ca data have been measured	Text	Selection from predefined list
Field added	*Ba_Ca_method*	Information on the measurement method for Ba/Ca	Text	Selection from predefined list
Field added	*Ba_Ca_std*	Information on the reference material used for Ba/Ca measurements	Text	Selection from predefined list
Field added	*Ba_Ca_downsampled*	Information on whether Ba/Ca data had to be downsampled	Text	Selection from predefined list
Field added	*Ba_Ca_downsampling_method*	Information on the downsampling method for Ba/Ca, if applicable	Text	Selection from predefined list
Field added	*U_Ca*	Indication of whether U/Ca data have been measured	Text	Selection from predefined list
Field added	*U_Ca_method*	Information on the measurement method for U/Ca	Text	Selection from predefined list
Field added	*U_Ca_std*	Information on the reference used for U/Ca measurements	Text	Selection from predefined list
Field added	*U_Ca_downsampled*	Information on whether U/Ca data had to be downsampled	Text	Selection from predefined list
Field added	*U_Ca_downsampling_method*	Information on the downsampling method for U/Ca, if applicable	Text	Selection from predefined list
Field added	*P_Ca*	Indication of whether P/Ca data have been measured	Text	Selection from predefined list
Field added	*P_Ca_method*	Information on measurement method for P/Ca	Text	Selection from predefined list

Table 2. Continued.

Action	Field label	Description	Format	Constraints
Field added	*P_Ca_std*	Information on the reference material used for P/Ca measurements	Text	Selection from predefined list
Field added	*P_Ca_downsampled*	Information on whether P/Ca data had to be downsampled	Text	Selection from predefined list
Field added	*P_Ca_downsampling_method*	Information on the downsampling method for P/Ca, if applicable	Text	Selection from predefined list
Field added	*Sr_isotopes*	Indication of whether Sr isotope data have been measured	Text	Selection from predefined list
Field added	*Sr_isotopes_method*	Information on the measurement method for Sr isotopes	Text	Selection from predefined list
Field added	*Sr_isotopes_std*	Information on the reference material used for Sr isotope measurements	Text	Selection from predefined list
Field added	*trace_elements_datafile*	Information on whether the original trace element data are available in the repository	Text	Selection from predefined list
Field added	*trace_elements_metadatafile*	Information on whether original trace element metadata are available in the repository	Text	Selection from predefined list
Field added	*cave_map*	Information on whether a copy of the cave map is available in the repository	Text	Selection from predefined list
Field added	*entity_scan*	Information on whether a scan of the speleothem is available in the repository	Text	Selection from predefined list
Changes made to the d18O and d13C tables				
Field removed	*iso_std*	Information on the reference material used for $\delta^{18}O$ and $\delta^{13}C$ measurements	Text	Selection from predefined list

topes and that the isotope sampling was continuous. Downsampling allows the trace element data to be represented by the same age–depth model as the stable isotope record. For records submitted by the authors in which the originally published dataset was at a higher resolution than reported in the SISAL database, standardized *.txt data files are also available in the repository (see Sect. 5.1 on code and data accessibility). No new chronological information or separate age models are reported for these datasets.

2.2 Additional metadata

New metadata fields are included in the Entity table (see the database structure in Fig. 1) to allow users to select sites with similar environmental conditions and to account for factors that might influence the interpretation of individual records. These include information on vegetation, land use, land cover, and host rock type above the cave. This information is often missing from publications and was not available from data contributors; therefore, information from data products has been added as additional fields to the database for completeness. Information on vegetation type and land use was provided by the original investigators. Additionally, information on land use and land cover was taken from the Copernicus Global Land Service Land Cover database (LCC v3.0.1; Epoch 2019; Buchhorn et al., 2021, 2020), extracted with a radius of 250 m around the cave site. Information on the carbonate/evaporite host rock at the cave sites was taken from the World Karst Aquifer Map (WoKAM) database (Goldscheider et al., 2020), extracted with a radius of 1000 m.

The database also indicates if the trace element content of the host rock and drip water feeding the speleothem is available (but does not include the actual values). Drip height (i.e. the distance the drip falls from the ceiling of the cave to the speleothem) and the difference between drip water and carbonate $\delta^{18}O$ values are given, based on information provided by the original investigators.

The SISAL WG repository now hosts images of the entities (speleothem sections) and maps of cave sites. These allow users to evaluate petrographic features that may influence the trace element and stable isotopic records and to check whether cave morphology could potentially influence the climate in the cave (Covington and Perne, 2015). The Entity table in the database contains fields indicating whether maps and images are available.

2.3 Changes to database structure

The structure of the SISALv3 database (Fig. 1) has been changed to accommodate additional data and metadata as well as to optimize the organization of information, as described below.

2.3.1 New geochemical data and metadata fields

The elemental ratio for each trace element and the Sr-isotope data are given in individual tables that contain sample identifiers (*sample_id*), the measurement value, and the measurement precision. The *sample_id* provides the link to the Sample table and, thus, links these data to the stable isotope data (Fig. 1, Table 2).

Metadata for the measurements are stored in the Entity table. For each elemental ratio (Sr/Ca, Mg/Ca, U/Ca, Ba/Ca, and P/Ca), the Entity table indicates whether the data are available ("yes/no/other/unknown"), the measurement method, the laboratory reference materials used, and (where applicable) the downsampling methods used. The table also indicates if high-resolution trace element data are available. For Sr isotopes, the Entity table specifies whether this dataset is available, what measurement method was employed, and how the measurement was standardized (Fig. 1, Table 2).

SISALv3 now provides a unique, persistent identifier for each speleothem (*persist_id*) in the Entity table (Fig. 1, Table 2). This was needed because there was an increasing issue with non-unique entity names; it was also required to deal with the fact that different datasets from the same stalagmite had different *entity_id* information (e.g. for datasets covering different time periods in the same speleothem). Thus, the field *entity_id* provides a unique identifier for a specific dataset, but not necessarily for a specific speleothem, while the *persist_id* uniquely identifies the speleothem. The *persist_id* information was created by combining the *site_id* and *entity_name* (without special characters). There are 838 unique *persist_id* entries and 902 unique *entity_id* entries in the database.

2.3.2 Changes in existing database fields and options

The fields "geology" and "rock age" were moved from the Site table to the Entity table (Fig. 1, Table 2). This was done to allow for variability in these parameters within the same cave system, which is particularly relevant for the interpretation of $\delta^{13}C$ and trace element data. The field "trace elements" (yes/no) in the Entity table was removed, as it was now redundant. The field "iso_std", describing the reference material used for the measurement of $\delta^{18}O$ and $\delta^{13}C$ values, was moved from the stable isotope tables to the Entity metadata table. A number of options for entries in the metadata fields were changed (Table 3). The majority of these changes were additions to the previously available options in light of the entries made in the "Notes" section to allow for more "metadata-filterable" database mining. A few options were removed from the metadata fields because they had never been used in previous database versions.

3 Quality control

The SISAL WG has used several levels of quality control (QC), and this practice was continued for SISALv3 (Fig. 2). The initial data compilation is performed by SISAL regional coordinators and/or in liaison with the data contributors into standardized Excel workbooks. The first QC level consists of expert assessment by the SISAL regional coordinators, who double-check the completeness of entered data and the correctness of measurement units where applicable. Standardized unit conversion sheets for common conversions (e.g. degrees–minutes–seconds to decimal degrees for site information, atomic ratios to activity ratios for dating information, or milligrams per gram to millimoles per mole for trace-element-to-Ca ratios for trace element information) have been provided to regional coordinators (see repository). The completed workbook(s) are subjected to a series of automated QC (e.g. checking if the age model matches the discreet dating information or if hiatuses are placed at the correct depth) by the database managers. When the datasets pass automated QC and no further corrections are necessary, the dataset workbook and the automatically generated QC figures are sent to the data contributors for final evaluation and approval. The same workflow has been followed for the *.txt trace element data files. The new metadata fields of vegetation_type and land_use have been added to SISALv3; for entities that were included in SISALv2, the information on these metadata fields has been added from publications. Data already included in SISALv2 have been checked, and mistakes or unknowns identified during previous data analysis or during the process of trace element data addition have been corrected. A comprehensive summary of the changes made

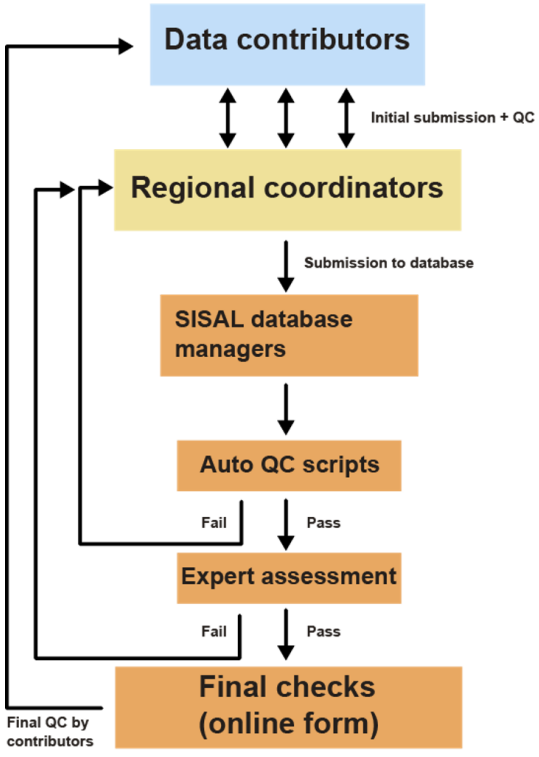

Figure 2. Quality checking workflow adopted for the inclusion of datasets in SISAL. The colours indicate different quality check levels: blue – data contribution sources (original authors or datasets deposited in repositories and publication supplementary information); yellow – SISAL regional coordinator group with regional expertise; orange – SISAL database managers.

Table 3. Changes made to the predefined options for metadata fields compared with SISALv2.

Table name	Action	Field label	Reason	Format	Constraints
Entity	Added "mixed (see notes)" option	*speleothem_type*	Standardization of option across fields	Text	Selected from predefined list
Entity	Added "other (see notes)" option	*speleothem_type*	Standardization of option across fields	Text	Selected from predefined list
Entity	Removed "magmatic" option	*geology*	Not used	Text	Selected from predefined list
Entity	Removed "granite" option	*geology*	Not used	Text	Selected from predefined list
Entity	Added "dolomite limestone" option	*geology*	Machine-readable format option	Text	Selected from predefined list
Entity	Added "marly limestone" option	*geology*	Machine-readable format option	Text	Selected from predefined list
Entity	Added "calcarenite" option	*geology*	Machine-readable format option	Text	Selected from predefined list
Entity	Added "other (see notes)" option	*geology*	Option to include free text in notes	Text	Selected from predefined list
Entity	Added "other (see notes)" option	*rock_age*	Option to include free text in notes	Text	Selected from predefined list
Entity	Added "mixed (see notes)" option	*rock_age*	Reflect overburden with rocks of different ages	Text	Selected from predefined list
Entity	Removed "mixture"	*drip_type*	Replaced with "mixed (see notes)" option	Text	Selected from predefined list
Entity	Removed "not applicable"	*drip_type*	Not used	Text	Selected from predefined list
Entity	Added "mixed (see notes)" option	*drip_type*	Standardization of option across fields	Text	Selected from predefined list
Entity	Added "other (see notes)" option	*drip_type*	Option to include free text in notes	Text	Selected from predefined list
Entity	Added "other (see notes)" option	*d18O_water_equilibrium*	Option to include free text in notes	Text	Selected from predefined list
Entity	Added "other (see notes)" option	*organics*	Option to include free text in notes	Text	Selected from predefined list
Entity	Added "other (see notes)" option	*fluid_inclusions*	Option to include free text in notes	Text	Selected from predefined list
Entity	Added "other (see notes)" option	*mineralogy_petrology_fabric*	Option to include free text in notes	Text	Selected from predefined list
Entity	Added "other (see notes)" option	*clumped_isotopes*	Option to include free text in notes	Text	Selected from predefined list
Entity	Added "other (see notes)" option	*noble_gas_temperatures*	Option to include free text in notes	Text	Selected from predefined list
Entity	Added "other (see notes)" option	*C14*	Option to include free text in notes	Text	Selected from predefined list
Entity	Added "other (see notes)" option	*ODL*	Option to include free text in notes	Text	Selected from predefined list
Dating	Added "mixed (see notes)" option	*material_dated*	Align with options in the Sample table	Text	Selected from predefined list
Dating_lamina	Added "Year of chemistry" option	*modern_reference*	Align with options in the Dating table	Text	Selected from predefined list
Sample	Removed "secondary calcite" option	*mineralogy*	Not used	Text	Selected from predefined list
Sample	Removed "vaterite" option	*mineralogy*	Not used	Text	Selected from predefined list
Sample	Added "organic" option	*mineralogy*	Addition of option	Text	Selected from predefined list
Sample	Added "other (see notes)" option	*mineralogy*	Option to include free text in notes	Text	Selected from predefined list
Sample	Removed "combination of methods" option	*age_model_type*	Standardization of option across fields	Text	Selected from predefined list
Sample	Added "mixed (see notes)" option	*age_model_type*	Standardization of option across fields	Text	Selected from predefined list
Sample	Added "other (see notes)" option	*dep_rate_check*	Option to include free text in notes	Text	Selected from predefined list

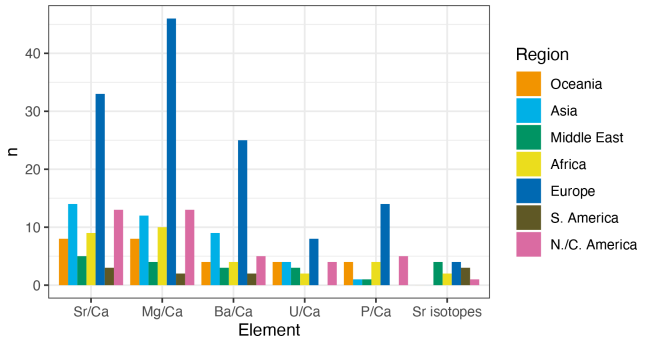

Figure 3. Trace element ratios and Sr-isotope records included in SISALv3 by region. Abbreviations: S. America – South America; N./C America – North and Central America.

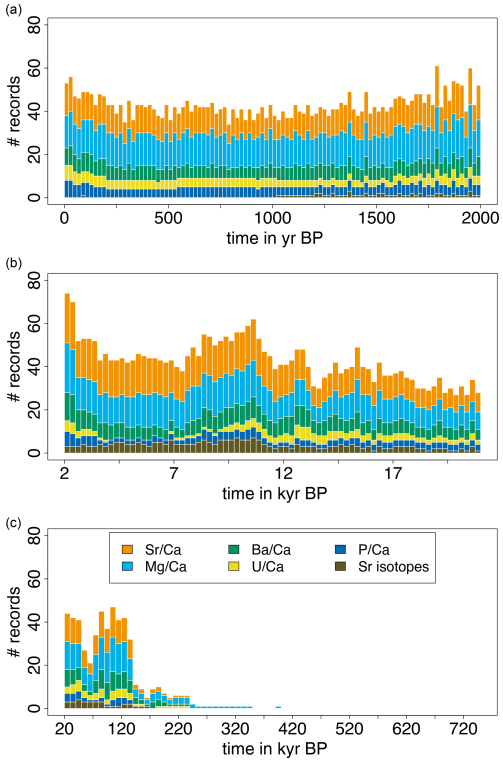

Figure 4. Temporal coverage of the trace element and Sr-isotope records in SISALv3 by region. Entities with multiple trace elements were counted multiple times. Bin sizes are as follows: **(a)** 0–2000 years BP – 20 years; **(b)** 2000–21 000 years BP – 250 years; **(c)** 21 000–750 000 years BP – 10 000 years.

to existing entities between SISALv2 and SISALv3 is shown in Table 4.

4 Overview of database contents

4.1 Trace element and Sr-isotope records

SISALv3 contains 95 Mg/Ca, 85 Sr/Ca, 52 Ba/Ca, 25 U/Ca, 29 P/Ca, and 14 Sr-isotope records (Table 5). This corresponds to ∼ 60 % of the known published data, based on an assessment by the SISAL WG. There is a clear regional bias in the database, with European entities dominating every elemental ratio (Fig. 3). The Sr-isotope records are more evenly distributed, with records from every region except Asia and Oceania. Temporal coverage for the combined trace element and Sr-isotope dataset is high during the last 2000 years (∼ 60 entities per 20-year interval) and the Holocene (∼ 60 entities per 250-year interval); it then drops to 20–40 entities per 10 000-year interval for the last glacial cycle (12–120 kyr BP, where "kyr" stands for 1000 years and BP for "before present", defined as 1950; Fig. 4). Beyond ∼ 120 kyr BP, the number of entities gradually decreases until the U–Th dating limit is reached (∼ 640 ka).

Where the original measured laser ablation data have been provided by data contributors, these have been made available as *.txt data files in the repository (Table 5). A total of 46 trace element records (15 Mg/Ca, 17 Sr/Ca, 4 Ba/Ca, 5 U/Ca, 5 P/Ca, and 2 Sr-isotope records) are only provided in the original format (*.txt files), either because they could not be converted to millimoles per mole or because the trace element data were not measured at stable-isotope-equivalent depths and were at an insufficiently high resolution for accurate resampling. Additional elements that are not included in the database but have been submitted by data contributors are also provided as *.txt files (e.g. Mn, Fe, Zn, Th, Pb, K, and Na).

4.2 New stable isotope records

SISALv3 provides a significantly expanded oxygen isotope dataset compared with SISALv2 (Tables 6, 7; Fig. 5), with 892 δ^{18}O records from 365 sites, compared with 673 records in SISALv2. The most significant increases in δ^{18}O records are in Africa (28 additional records), Europe (73 additional records), and Asia (50 additional records; Table 6). SISALv3 contains 334 entities covering the last 2000 years, of which 78 are new (Fig. 6). As record density begins to decrease with age (Fig. 6), the spatial distribution is reduced as well. For the Last Glacial Maximum (20–22 kyr BP), SISALv3 contains 92 entities (11 new), while for the Last Interglacial (124–126 kyr BP), 66 entities are available (15 new). Four δ^{18}O records previously included in SISALv2 have been modified to correct previous mistakes (Table 4); these are *entity_id* 110 (CUR4; Novello et al., 2016), 169 (Dim-E3; Ünal-İmer et al., 2015), 447 (JAR4; Novello et al., 2017), and 573 (Gej-1; Flohr et al., 2017).

There has also been a significant increase in the number of δ^{13}C records added, with 620 records in SISALv3 compared with 430 in SISALv2 (Table 6, Fig. 7). At the regional scale, the most significant increases in δ^{13}C records are for Africa (23 additional records), Asia (33 additional records), and Europe (66 additional records; Table 6). The δ^{13}C record coverage decreases following the same patterns as the trace element and δ^{18}O records (Fig. 8). Two δ^{13}C records pre-

Table 4. Summary of the modifications applied to records in version 2 (Comas-Bru et al., 2020) of the SISAL database. Note that the changes in the Dating table and the Sample table were counted by dating_id and sample_id, respectively, which led to a large number of changes.

Modification	v2 to v3
Site table	
Number of new sites	72
Pre-existing sites with new entities	37
Entity table	
Number of new entities	211
Entities added to pre-existing sites	71
Entities with updated entity.entity_status	33
Entities with altered entity.corresponding_current	1
Entities with altered geology	106
Entities with altered rock_age	58
Entities with altered entity.cover_thickness	6
Entities with altered distance_entrance	1
Entities with altered d13C	109
Entities with altered d18O	15
Entities with altered organics	9
Entities with altered fluid_inclusions	9
Entities with altered mineralogy_petrology_fabric	14
Entities with altered clumped_isotopes	9
Entities with altered noble_gas_temperatures	12
Entities with altered C14	3
Entities with altered ODL	7
Entities with altered contact	62
Entities with altered data_DOI_url	20
Dating table	
Addition of "event: hiatus" to an entity	1
Changes in hiatus depths	1
Changes in depths of "Event: start/end of laminations"	1
Alterations in dating.date_type	2
Alterations in dating.depth_dating	5
Alterations in dating.material_dated	2
Alterations in dating.min_weight	6
Alterations in dating.max_weight	6
Alterations in dating.uncorr_age	15
Alterations in dating.uncorr_age_uncert_pos	13
Alterations in dating.uncorr_age_uncert_neg	13
Alterations in dating.date_used	27
Alterations in dating.238U_content	89
Alterations in dating.238U_uncertainty	34
Alterations in dating.232Th_content	96
Alterations in dating.232Th_uncertainty	85
Alterations in dating.230Th_232Th_ratio	206
Alterations in dating.230Th_232Th_ratio_uncertainty	200
Alterations in dating.230Th_238U_activity	24
Alterations in dating.230Th_238U_activity_uncertainty	21
Alterations in dating.234U_238U_activity	381
Alterations in dating.234U_238U_activity_uncertainty	433
Alterations in dating.ini_230Th_232Th_ratio	519
Alterations in dating.ini_230Th_232Th_ratio_uncertainty	485
Alterations in dating.decay_constant	77
Alterations in dating.corr_age	71
Alterations in dating.corr_age_uncert_pos	26
Alterations in dating.corr_age_uncert_neg	28

Table 4. Continued.

Modification	v2 to v3
Sample table	
Altered sample.depth_sample	1084
Altered sample.mineralogy	294
Altered sample.arag_corr	294
Entities that had d18O time series altered (changes in depth/ duplicate isotope values)	4
Entities that had d13C time series altered (changes in depth/ duplicate isotope values)	2
Original chronology	
Altered original_chronology.interp_age	7440
References	
How many entities had changes in references?	100
How many citations have a different pub_DOI?	100
Notes	
Sites with notes modified	121

Table 5. Summary of the number of trace element records in SISAL and the downsampling methods applied.

Geochemical data	Total number in SISAL	Downsampled by original authors	Downsampled by SISAL	Only in repository
Mg/Ca	95	12	15	15
Sr/Ca	85	11	11	17
Ba/Ca	52	11	9	4
U/Ca	25	2	6	5
P/Ca	29	4	12	5

Table 6. Summary of the new δ^{18}O and δ^{13}C records added to SISALv3 compared with SISALv2.

Region	δ^{18}O records in v3	Increase compared with v2 (counts)	δ^{13}C records in v3	Increase compared with v2 (counts)
Africa	73	28	63	23
Asia	237	50	105	33
Europe	243	73	213	66
Middle East	60	17	43	14
Oceania	100	11	66	11
North and Central America	88	9	72	9
South America	97	21	54	13

viously included in SISALv2 have been modified to correct previous mistakes (Table 4); these are *entity_id* 169 (Dim-E3; Ünal-İmer et al., 2015) and 573 (Gej-1; Flohr et al., 2017).

4.3 Vegetation and land cover metadata

Interpretation of the site-to-site variability in speleothem data sensitive to vegetation changes is facilitated by providing information on *vegetation_type* and *land_use*. The dropdown list for these fields includes options typically used in speleothem publications. Additional information provided by the authors (e.g. species names) has been added to the Notes table. About 40 % of the database entries lack the author-reported information on land cover (Fig. 9c). Satellite-derived land cover classifications provide information for many more sites (unknown: 1.7 %; Fig. 9d). Forested sites (evergreen, deciduous, and mixed) comprise ∼ 56.5 % (Fig. 9d), shrub- and grassland make up 25.1 %, and this dataset also denotes sites that are affected by anthropogenic

Table 7. New entities added to SISALv3.

site_id	site_name	region	latitude	longitude	persist_id	entity_id	entity_name	citation
70	Abaco Island Cave	The Bahamas	26.23	−77.16	70-ABDC12	692	AB-DC-12_2023	Arienzo et al. (2017)
79	Dim Cave	Türkiye	36.534	32.1056	79-DIME4	693	Dim-E4_2023	Ünal-İmer et al. (2016, 2015)
					79-DIM1	754	Dim1	Rowe et al. (2020)
144	Botuverá Cave	Brazil	−27.2247	−49.1569	144-BT2	694	BT-2_2007	Cruz et al. (2007)
145	Antro del Corchia	Italy	43.9833	10.2167	145-CD31	695	CD3-1_HR	Drysdale et al. (2020)
						696	CD3-1_LR	Drysdale et al. (2020)
266	Cueva Victoria	Spain	37.6322	−0.8215	266-VICIII1	697	Vic-III-1	Budsky et al. (2019); Ros and Llamusí (2012)
					266-VICIII3	698	Vic-III-3	Budsky et al. (2019); Ros and Llamusí (2012)
					266-SR01T	699	SR01t	Budsky et al. (2019); Ros and Llamusí (2012)
39	Dongge Cave	China	25.2833	108.0833	39-D3	700	D3_2005	Kelly et al. (2006)
					39-D4	701	D4_2005_Kelly	Kelly et al. (2006)
120	Ejulve Cave	Spain	40.76	−0.59	120-ANDROMEDA	702	Andromeda	Pérez-Mejías et al. (2019)
192	El Condor Cave	Peru	−5.93	−77.3	192-ELCB	703	ELC-B_2021	Cheng et al. (2021)
115	Hölloch im Mahdtal	Austria	47.3781	10.1506	115-HOL1	704	HOL1	H. Li et al. (2021)
					115-HOL22	705	HOL22	H. Li et al. (2021)
6	Hulu Cave	China	32.5	119.17	6-MSL	706	MSL_2021	Cheng et al. (2021)
10	Jaraguá Cave	Brazil	−21.083	−56.583	10-JAR2	707	JAR2	Novello et al. (2019)
24	Lapa Sem Fim Cave	Brazil	−16.1503	−44.6281	24-LSF13	708	LSF13_2018	Stríkis et al. (2018)
					24-LSF19	709	LSF19	Azevedo et al. (2021)
					24-LSF17	710	LSF17	Azevedo et al. (2021)
					24-LSF13	711	LSF13_2021	Cheng et al. (2021)
3	Paraiso Cave	Brazil	−4.0667	−55.45	3-PAR27	712	PAR27	Cheng et al. (2021)
					3-PAR15	713	PAR15	Cheng et al. (2021)
268	Pere Noel Cave	Belgium	50	5.2	268-PN955	714	PN-95-5_2018	Allan et al. (2018) Allan et al. (2018)
87	Pindal Cave	Spain	43.4	−4.53	87-CANDELA	715	Candela_2023	Moreno et al. (2010)
						716	Candela_Base	Stoll et al. (2022)
						717	Candela_Main	Stoll et al. (2022)
						718	Candela_L	Stoll et al. (2022)
					87-LAURA	719	Laura	Stoll et al. (2022)
295	Qadisha Cave	Lebanon	34.2439	30.0364	295-QAD1	720	Qad_1	Nehme et al. (2023)
					295-QAD2	721	Qad_2	Nehme et al. (2023)
232	Rio Secreto cave system	Mexico	20.59	−87.13	232-RS1	722	RS1	Serrato Marks et al. (2021)
219	Shennong Cave	China	28.71	117.26	219-SN35	723	SN35	Zhang et al. (2021c)
					219-SN31	724	SN31	Zhang et al. (2021c)
					219-SN29	725	SN29	Zhang et al. (2021c)
					219-SN-COMP	726	SN_composite	Zhang et al. (2021c)
					219-SN17	727	SN17_2021	Zhang et al. (2021c)
55	Sieben Hengste Cave	Austria	46.75	7.81	55-7H12	728	7H-12	Luetscher et al. (2021)
58	Spannagel Cave	Austria	47.08	11.67	58-SPA121	729	SPA121_2021	Wendt et al. (2021)
					58-SPA146	730	SPA146	Wendt et al. (2021)
					58-SPA183	731	SPA183	Wendt et al. (2021)
					58-SPA127	732	SPA127_2023	Fohlmeister et al. (2013), Welte et al. (2021)
279	Staircase Cave	South Africa	−34.2071	22.0899	279-STAIRCASE-COMP	733	Staircase_composite	Braun et al. (2019a)

Table 7. Continued.

site_id	site_name	region	latitude	longitude	persist_id	entity_id	entity_name	citation
236	Toca da Boa Vista	Brazil	−10.1602	−40.8605	236-TBV5	734	TBV5	Cheng et al. (2021)
					236-TBV13	735	TBV13	Zhang et al. (2021b)
69	Xinglong Cave	China	40.5	117.5	69-XL4	736	XL-4	Duan et al. (2019, 2022)
296	Amir Timur Cave	Uzbekistan	39.4227	66.7632	296-S124	737	S-12-4	Finestone et al. (2022)
94	Anjohibe	Madagascar	−15.53	46.88	94-ABC1	738	ABC-1	Li et al. (2020)
297	Bàsura Cave	Italy	44.13	8.2	297-BA184	739	BA18-4	Hu et al. (2022)
298	Belum Cave	India	15.1	78.1	298-BLM1	740	BLM-1	Band et al. (2022)
299	Calabrez	Spain	43.45	−5.13	299-ALICIA	741	Alicia	Stoll et al. (2022)
300	Careys Cave	Australia	−35.07	148.66	300-CC146	742	CC14-6	Scroxton et al. (2021)
301	Cathedral Cave	Australia	−32.617	148.94	301-WB	743	WB	Markowska et al. (2020)
					301-WC	744	WC	Markowska et al. (2020)
302	Crevice Cave	South Africa	−34.21	22.09	302-CREVICE-COMP	745	Crevice_composite	Bar-Matthews et al. (2010)
303	Crystal Cave	Australia	−34.1	115	303-CRYS1	746	CRY-S1	Priestley et al. (2023), Treble et al. (2003)
304	Cueva Bonita	Mexico	23	−99	304-CB4	747	CB4	Wright et al. (2022)
305	Cueva Rosa	Spain	43.4436	−5.1403	305-NEITH	748	Neith_2022	Stoll et al. (2022)
						749	Neith_2015	Stoll et al. (2015)
					305-ARTEMISAR	750	Artemisa_R	Stoll et al. (2015)
					305-ANGELINES	751	Angelines	Stoll et al. (2015)
306	Cuíca Cave	Brazil	−11.6822	−60.6431	306-PIM4	752	PIM4	Della Libera et al. (2022)
					306-PIM5	753	PIM5	Della Libera et al. (2022)
307	Efflux Cave	South Africa	−33.41	22.34	307-EFFLUX-COMP	755	Efflux_composite	Braun et al. (2020)
					307-142843	756	142843	Braun et al. (2020)
					307-142846	757	142846	Braun et al. (2020)
					307-142847	758	142847	Braun et al. (2020)
					307-142848	759	142848	Braun et al. (2020)
					307-142849	760	142849	Braun et al. (2020)
308	GD8	Greenland	80.3777	−21.7468	308-GD81SLAB1	761	GD8-1 Slab 1	Moseley et al. (2021)
					308-GD81SLAB1ORB	762	GD8-1 Slab 1 orb	Moseley et al. (2021)
					308-GD81SLAB2	763	GD8-1 Slab 2	Moseley et al. (2021)
309	Goda Mea Cave	Ethiopia	9.49	37.66	309-GM1	764	GM1	Asrat et al. (2018)
310	Golgotha Cave	Australia	−34.083	115.05	310-GLS1	765	GL-S1	Treble et al. (2022)
					310-GLS2	766	GL-S2	Treble et al. (2022)
					310-GLS3	767	GL-S3	Treble et al. (2022)
					310-GLS4	768	GL-S4	Treble et al. (2022)
311	Harrie Wood Cave	Australia	−35.7	148.5	311-HWS1	769	HW-S1	Tadros et al. (2022, 2016)
					311-HWS2	770	HW-S2	Tadros et al. (2022, 2016)
					311-HW38B	771	HW_38b	Tadros et al. (2022, 2016)
312	Heifeng Cave	China	29.0167	107.1833	312-HF01	772	HF01	Yang et al. (2019)
313	Herbstlabyrinth Cave	Germany	50.6875	8.2058	313-HLK2	773	HLK2	Waltgenbach et al. (2020)
					313-NG01	774	NG01	Waltgenbach et al. (2021)
					313-TV1	775	TV1_2021	Waltgenbach et al. (2021)
						776	TV1_2020	Waltgenbach et al. (2020)

Table 7. Continued.

site_id	site_name	region	latitude	longitude	persist_id	entity_id	entity_name	citation
314	Herolds Bay Cave	South Africa	−34.05	22.39	314-HEROLDSBAY-COMP	777	Herolds_bay_composite	Braun et al. (2020)
					314-162520	778	162520	Braun et al. (2020)
					314-1625271	779	162527-1	Braun et al. (2020)
					314-162528	780	162528	Braun et al. (2020)
					314-1625272	781	162527-2	Braun et al. (2020)
315	Huangchao Cave	China	36.6167	118.3333	315-HC2	782	HC2	Tan et al. (2020b)
316	Hüttenbläser-schacht-höhle	Germany	51.3689	7.6547	316-HBSH1	783	HBSH-1	Weber et al. (2021)
					316-HBSH3	784	HBSH-3	Weber et al. (2021)
					316-HBSH4	785	HBSH-4	Weber et al. (2021)
					316-HBSH5	786	HBSH-5	Weber et al. (2021)
42	Ifoulki Cave	Morocco	30.708	−9.3275	42-IFK2	787	IFK2	Sha et al. (2021)
317	Jiangjun Cave	China	22.95	104.8167	317-JJ0406	788	JJ0406	Wassenburg et al. (2021); Liu et al. (2020)
					317-JJ0403	789	JJ0403	Wassenburg et al. (2021); Liu et al. (2020)
318	Jinfo Cave	China	29.0167	107.1792	318-J12	790	J12	Yang et al. (2019)
					318-J13	791	J13	Yang et al. (2019)
319	Jiulong Cave	China	27.8	113.9	319-JL1	792	JL1	Zhang et al. (2021a)
320	Katalekhor	Iran	35.85	48.16	320-KT3	793	KT-3	Andrews et al. (2020)
100	Katerloch Cave	Austria	47.0833	15.55	100-K2	794	K2	Honiat et al. (2022)
					100-K4	795	K4	Honiat et al. (2022)
321	Klang Cave	Thailand	8.33	98.73	321-TK7	796	TK7	Chawchai et al. (2021)
					321-TK20	797	TK20	Chawchai et al. (2021)
					321-TK40	798	TK40	Chawchai et al. (2021)
322	Kuna Ba Cave	Iraq	35.09	45.38	322-NIR1	799	NIR-1	Sinha et al. (2019)
					322-NIR2	800	NIR-2	Sinha et al. (2019)
					322-NIR-COMP	801	NIR_composite	Sinha et al. (2019)
323	Kyok-Tash Cave	Russia	51.729	85.656	323-K4KYOK	802	K4_kyok	T.-Y. Li et al. (2021)
324	La Vallina Cave	Spain	43.41	−4.8067	324-GAEL	803	Gael_2022	Stoll et al. (2022)
						804	Gael_2015	Stoll et al. (2015)
					324-GLORIA	805	Gloria	Stoll et al. (2015)
					324-GARTH	806	Garth	Stoll et al. (2022)
					324-GULDA	807	Gulda	Stoll et al. (2022)
					324-LUNA	808	Luna	Stoll et al. (2022)
					324-GALIA	809	Galia	Stoll et al. (2022)
221	La Vierge Cave	Mauritius	−19.7572	63.3703	221-LAVI157	810	LAVI-15-7	Li et al. (2020)
					221-LAVI4	811	LAVI-4_2020	Li et al. (2020)
325	Larga Cave	Puerto Rico	18.32	−66.8	325-PRLA1	812	PR-LA-1	Warken et al. (2020)
326	Linzhu Cave	China	31.5167	110.3167	326-LZ15	813	LZ15	Cheng et al. (2009a)
					326-LZ36	814	LZ36	Cheng et al. (2009a)
327	Manita peć Cave	Croatia	45.3142	15.4754	327-MP2	815	MP-2	Surić et al. (2021b)
					327-MP3	816	MP-3	Surić et al. (2021b)
328	Mata Virgem Cave	Brazil	−11.62	−47.49	328-MV3	817	MV3	Azevedo et al. (2019)
329	Matupi Cave	Democratic Republic of Congo	1.25	29.82	329-MAT1	818	MAT1	Dupont et al. (2022)
					329-MAT12	819	MAT12	Dupont et al. (2022)
					329-MAT23	820	MAT23	Dupont et al. (2022)
330	Meravelles Cave	Spain	40.9488	0.5127	330-MAAT	821	Maat	Pérez-Mejías et al. (2021)

Table 7. Continued.

site_id	site_name	region	latitude	longitude	persist_id	entity_id	entity_name	citation
331	Mizpe Shelagim	Mount Hermon (Levant)	33.32	35.81	331-MS-COMP	822	MS-composite	Ayalon et al. (2013)
					331-MS1	823	MS-1	Ayalon et al. (2013)
					331-MS2	824	MS-2	Ayalon et al. (2013)
					331-MS3	825	MS-3	Ayalon et al. (2013)
332	Murada	Spain	39.956	3.965	332-INDIANA	826	Indiana	Torner et al. (2019)
333	Neotektonik Cave	Switzerland	46.7833	8.2667	333-M37116A	827	M37-1-16A	Wilcox et al. (2020)
					333-M37116C	828	M37-1-16C	Wilcox et al. (2020)
					333-M37123A	829	M37-1-23A	Wilcox et al. (2020)
334	Nova Grgosova Cave	Croatia	45.8188	15.6783	334-NG7	830	NG-7	Surić et al. (2021a)
					334-NG3	831	NG-3	Surić et al. (2021a)
335	Ostolo Cave	Spain	43.1878	−0.2678	335-OST2	832	OST2	Bernal-Wormull et al. (2021)
					335-OST1	833	OST1	Bernal-Wormull et al. (2021)
					335-OST3	834	OST3	Bernal-Wormull et al. (2021)
336	Pentadactylos	Cyprus	35.27	33.47	336-PENTADACTYLOS1	835	Pentadactylos-1	Nehme et al. (2020)
337	Pir Ghar Cave	Iran	35.23	57.42	337-PG113	836	PG11-3	Carolin et al. (2019a)
338	Coves del Pirata	Spain	39.5046	3.3009	338-CONSTANTINE	837	Constantine	Cisneros et al. (2021)
339	Pozzo Cucù Cave	Italy	40.9	17.16	339-PC	838	PC	Columbu et al. (2020)
254	PP29	South Africa	−34.2078	22.0876	254-PP29-COMP	839	PP29_composite	Braun et al. (2019a)
340	Qujia Cave	China	35.7	118.4	340-QJ1	840	QJ1	Zhao et al. (2021)
341	Rey Marcos	Guatemala	15.4277	−90.2807	341-GURM1	841	GU-RM-1	Winter et al. (2020)
342	Sa balma des Quartó Cave	Spain	39.5145	3.3059	342-SEAN	842	Seán	Cisneros et al. (2021)
					342-MULTIEIX	843	Multieix	Cisneros et al. (2021)
					342-CIARA	844	Ciara	Cisneros et al. (2021)
					342-FENI	845	Feni	Cisneros et al. (2021)
140	Sanbao Cave	China	31.667	110.4333	140-SB61	846	SB61	Cheng et al. (2009a)
343	Sant'Angelo Cave	Italy	40.7	17.5	343-SA1	847	SA1	Columbu et al. (2022)
345	Schratten Cave	Switzerland	46.7833	8.2667	345-M6733	849	M6-73-3	Wilcox et al. (2020)
20	Secret Cave	Borneo	4.0848	114.8503	20-SC02	850	SC02_2022	Buckingham et al. (2022)
346	Shijiangjun Cave	China	26.2	105.5	346-SJJ7	851	SJJ7	Chen et al. (2021)
347	Shizi Cave	China	29.6822	106.2881	347-QM09	852	QM09	Yang et al. (2019)
348	Sudwala Cave	South Africa	−25.37	20.7	348-SC1	853	SC1	Green et al. (2015)
349	Talisman Cave	Kyrgyzstan	40.39	72.35	349-F11	854	F11	Tan et al. (2021)
					349-F2TALISMAN	855	F2_Talisman	Tan et al. (2021)
293	Tham Doun Mai Cave	Laos	20.75	102.65	293-TM5	856	TM5	Griffiths et al. (2020)
				102.65	293-TM4	857	TM4	Griffiths et al. (2020)
				102.65	293-TM11	858	TM11	Griffiths et al. (2020)
350	Toca da Barriguda	Brazil	−10.16	−40.86	350-TBR14	859	TBR14	Wendt et al. (2019)
					350-TBR1013	860	TBR10-13	Cheng et al. (2021)
351	Trapiá Cave	Brazil	−5.6	−37.7	351-TRA7	861	TRA7	Utida et al. (2020)
352	War Eagle	USA	34.67	−86.05	352-PPNDA	862	PPnda	Medina-Elizalde et al. (2022)

Table 7. Continued.

site_id	site_name	region	latitude	longitude	persist_id	entity_id	entity_name	citation
250	Wuya Cave	China	33.82	105.43	250-WY12	863	WY12	Tan et al. (2020a)
					250-WY13	864	WY13	Tan et al. (2020a)
					250-WY14	865	WY14	Tan et al. (2020a)
					250-WY56	866	WY56	Tan et al. (2020a)
353	Wintimdouine	Morocco	30.77	−9.49	353-WIN1	867	WIN1	Sha et al. (2019)
					353-WIN2	868	WIN2	Sha et al. (2021, 2019)
					353-WIN3	869	WIN3	Sha et al. (2021, 2019)
					353-WIN-COMP	870	WIN_composite	Sha et al. (2019)
354	Wulu Cave	China	26.05	105.0833	354-WULU30	871	Wulu-30	Cheng et al. (2021), Liu et al. (2018)
					354-WU88	872	Wu88	Liu et al. (2023, p. 202)
					354-WU37	873	Wu37	Zhao et al. (2020)
355	Xiniu Cave	China	31.5167	110.57	355-XN2	874	XN2	Zhao et al. (2021)
				110.57	355-XN15	875	XN15	Zhao et al. (2021)
				110.57	355-XN-COMP	876	XN_composite	Zhao et al. (2021)
5	Yangkou Cave	China	29.0333	107.1833	5-JFYK2	877	JFYK2	Zhang et al. (2021a)
356	Yangzi Cave	China	29.783	107.783	356-YZ1	878	YZ1	Wu et al. (2020)
357	Yonderup Cave	Australia	−31.547	115.69	357-YDS2	879	YD-S2	McDonough et al. (2022); Nagra et al. (2017, 2016)
358	Zhangjia Cave	China	32.5833	105.0833	358-ZJD171	880	ZJD171	Cheng et al. (2021)
359	Zoolithen Cave	Germany	49.7793	11.2829	359-ZOOREZ1	881	Zoo-rez-1	Riechelmann et al. (2019, 2020)
					359-ZOOREZ2	882	Zoo-rez-2	Riechelmann et al. (2019, 2020)
360	Bigonda Cave	Italy	46.018	11.581	360-BG2	883	BG2	Johnston et al. (2021)
					360-BG4	884	BG4	Johnston et al. (2021)
117	Bunker Cave	Germany	51.3675	7.6647	117-BU1	885	Bu1_2021	Waltgenbach et al. (2021)
					117-BU4	886	Bu4_2021	Waltgenbach et al. (2021, 2020)
361	Kocain Cave	Türkiye	37.2325	30.7117	361-KO1	887	Ko-1	Jacobson et al. (2021)
362	Labyrinth Cave	Australia	−34.3	115.1	362-LABS1	888	LAB-S1	Nagra et al. (2017), Priestley et al. (2023)
363	Lake Shasta Cave	USA	40.804	−122.304	363-LSC2	889	LSC2	Oster et al. (2020)
					363-LSC3	890	LSC3	Oster et al. (2020)
12	Mawmluh Cave	India	25.2622	91.8817	12-MAW3	891	MAW-3	Magiera et al. (2019)
364	Naharon	Mexico	20.18	−87.54	364-NAH14	892	NAH14	Warken et al. (2021)
365	Pot au Feu	Spain	42.52	0.24	365-JUD	893	JUD	Torner et al. (2019)
366	Savi Cave	Italy	45.6167	13.8833	366-SV1	894	SV1	Belli et al. (2013, 2017)
					366-SV7	895	SV7	Belli et al. (2013, 2017)
205	São Bernardo Cave	Brazil	−13.81	−46.35	205-SBE3	896	SBE3_2021	Novello et al. (2018, 2021)
225	Chiflonkhakha Cave	Bolivia	−18.1222	−65.7739	225-BOTO1	897	Boto 1_2021	Apaéstegui et al. (2018); Novello et al. (2021)
					225-BOTO3	898	Boto 3_2021	Apaéstegui et al. (2018); Novello et al. (2021)
					225-BOTO7	899	Boto 7_2021	Apaéstegui et al. (2018); Novello et al. (2021)
54	Sahiya Cave	India	30.6	77.8667	54-SAHA	900	SAH-A_2023	Sinha et al. (2015)
					54-SAHB	901	SAH-B_2023	Sinha et al. (2015)
					54-SAHAB-COMP	902	SAH-AB_2023	Sinha et al. (2015)
344	Sarma Cave	Republic of Abkhazia (Caucasus)	−25.37	20.7	344-SAR121	848	SAR-12-1	Wolf et al. (2024)

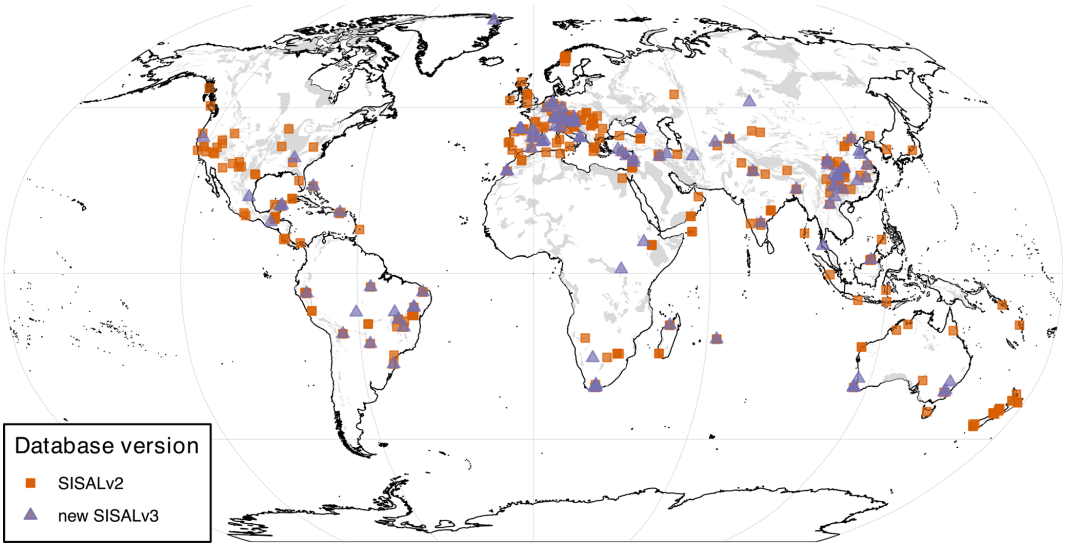

Figure 5. Global map of $\delta^{18}O$ records included in SISAL v2 and v3. The shaded background shows the global karst distribution extracted from the World Karst Aquifer Map (WoKAM; Goldscheider et al., 2020).

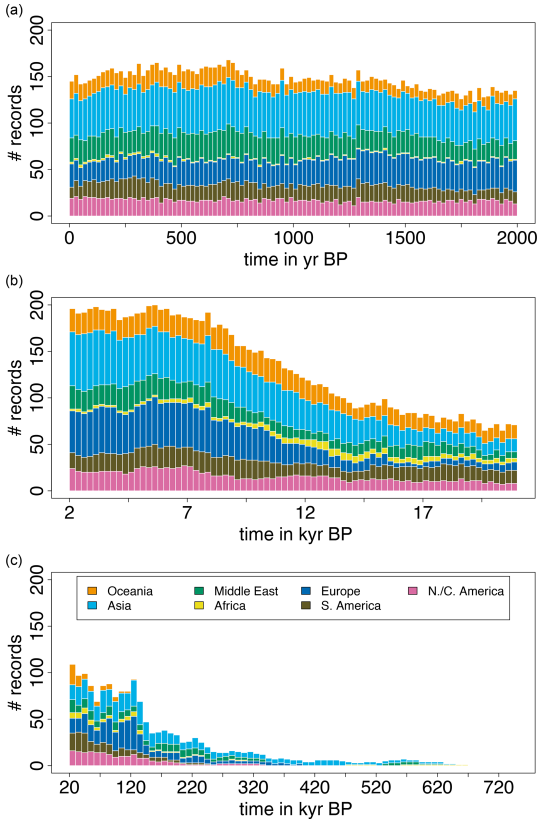

Figure 6. Temporal coverage of the $\delta^{18}O$ records in SISALv3 by region. Bin sizes are as follows: **(a)** 0–2000 years BP – 20 years; **(b)** 2000–21 000 years BP – 250 years; **(c)** 21 000–750 000 years BP – 10 000 years.

land use (managed vegetation, agriculture, and urban), which make up 13 %.

5 Recommendations for use

The SISALv3 database is a standardized, quality-checked dataset that allows regional to global assessments of spatial and temporal trends in multiple environmental proxies from speleothem records. The addition of trace element data at stable-isotope-equivalent depths to the database and machine-readable metadata fields allow the examination of hydroclimatic controls on the speleothem trace element distribution. Metadata fields, including distance from coast (*latitude, longitude*, and *elevation*), lithology (*geology* and *wokam*), and land cover (*cover_type*, *cover_thickness, vegetation_type, land_use*, and *copernicus_lcc*), allow the identification of the primary controls on trace elements. We recommend using multiple cover fields together, based on the analysis type and scope (e.g. time interval considered), as they provide complementary information. Anthropogenic and natural changes in the cover parameters over time need to be considered, and this applies particularly for the cover fields *vegetation_type*, *land_use*, and *copernicus_lcc*, which (in most cases) may only be applicable for very recent speleothem growth.

Where trace elements are measured on aliquots of the same powder as stable isotopes, the sample-to-sample variability in depth–time space is minimal. Where samples for stable isotopes and trace elements have been drilled at different times or in situ methods have been used for trace element measurements, there may be depth–time variability that may impact the results. Extensive metadata on sampling and measurement methods as well as the original high-

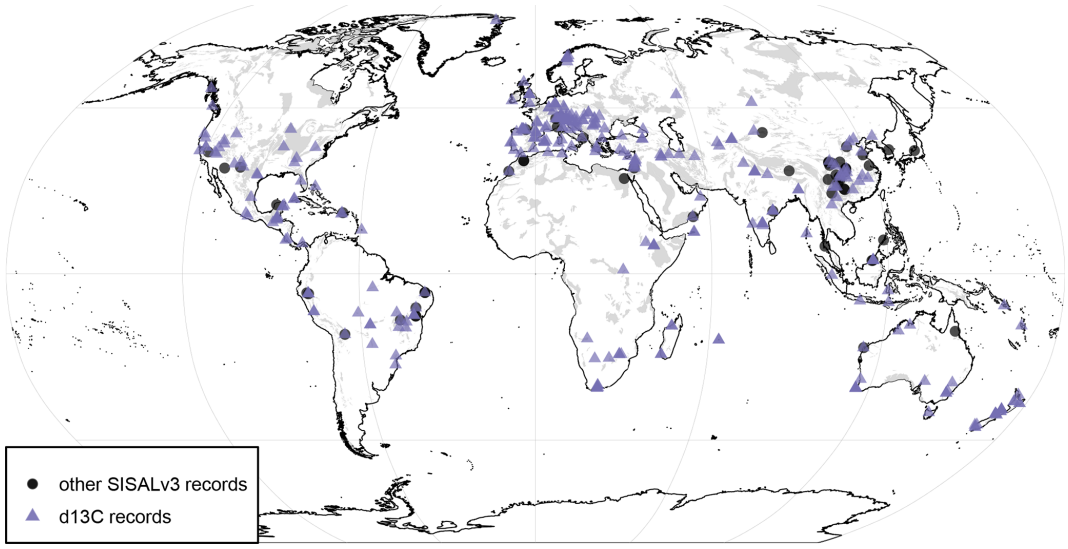

Figure 7. Map of available $\delta^{13}C$ records in SISALv3 compared with all records in the database. The shaded background shows the global karst distribution extracted from the World Karst Aquifer Map (WoKAM; Goldscheider et al., 2020).

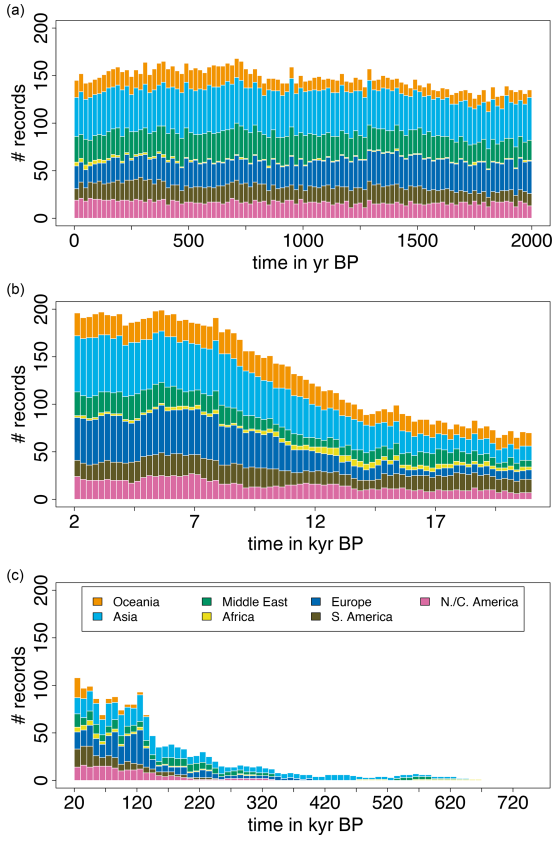

Figure 8. Temporal coverage of the $\delta^{13}C$ records in SISALv3 by region. Bin sizes are as follows: **(a)** 0–2000 years BP – 20 years; **(b)** 2000–21 000 years BP – 250 years; **(c)** 21 000–750 000 years BP – 10 000 years.

resolution in situ measurements against depth are provided in the database and linked repository and should be used to check for such impacts. Measurements may also be sensitive to stalagmite petrography; image scans have been provided in the linked repository so that the user can evaluate whether this is important for the interpretation of the record.

5.1 Code and data availability

The database is available in CSV and SQL format in a repository at https://doi.org/10.5287/ora-2nanwp4rk (Kaushal et al., 2024). This dataset is licensed by the rights holder(s) under a Creative Commons Attribution 4.0 International licence: https://creativecommons.org/licenses/by/4.0/ (last access: 8 March 2024). Apart from the workbook used to submit data to the SISAL database and the codes for automatic quality checking, the repository contains additional standardization sheets (coordinate conversion, grams to moles conversion for trace elements, and atomic activity calculator for U-series data). Moreover, the repository contains all submitted cave maps and entity images in separate zip folders as well as copyright information for the individual images and an entity scan "wish list" that details best practices for entity scan images. Standardized trace element data files are included separately with their metadata (see Sect. 2) and the codes needed to connect and use the database (described in the README file).

The codes for standardization and downsampling of trace element and Sr-isotope records are available at Zenodo (https://doi.org/10.5281/zenodo.8234066, Skiba, 2023; licensed by the right holder(s) under Creative Commons Attribution 4.0 International).

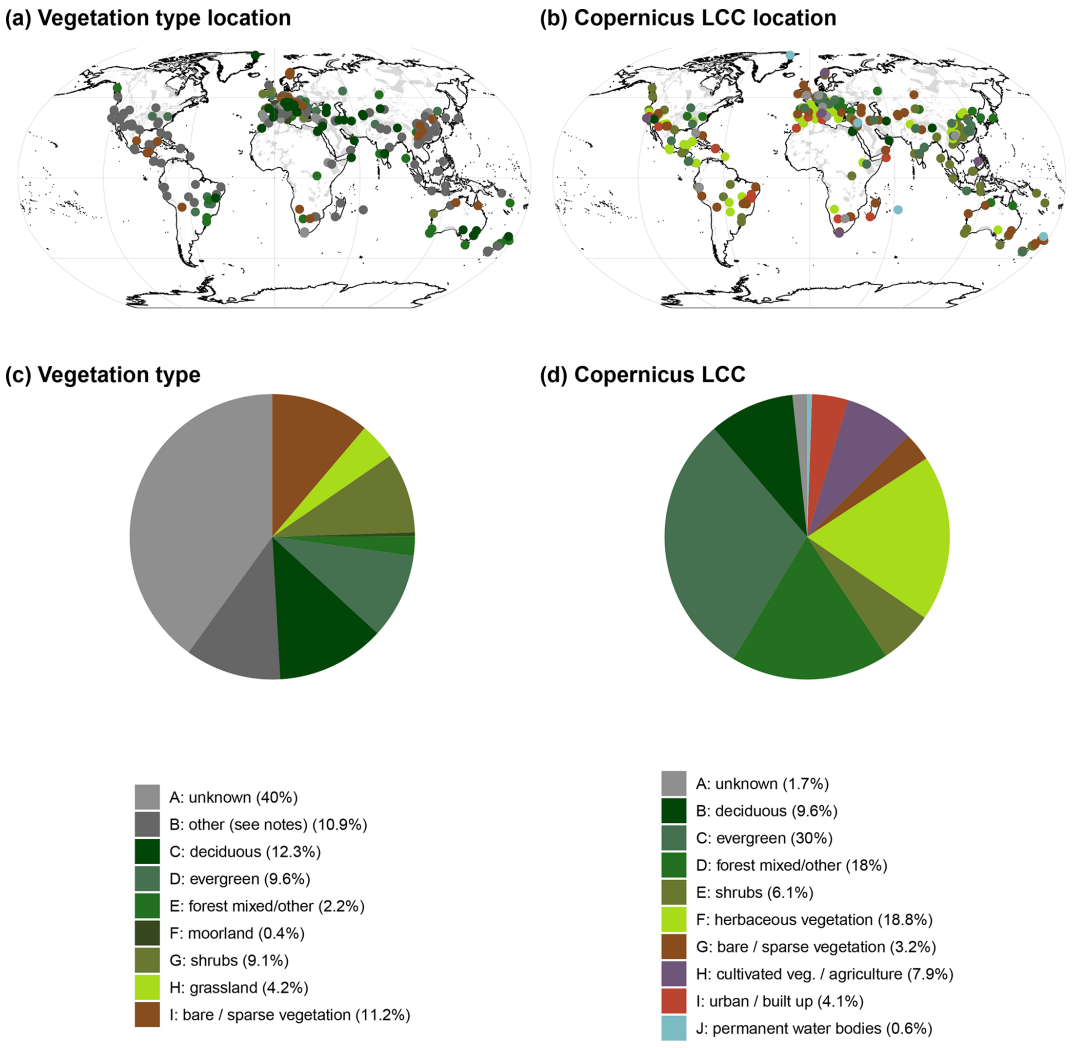

Figure 9. **(a)** Vegetation description from the original publications or provided by authors and **(b)** land cover categories extracted from the Copernicus LCC database (Buchhorn et al., 2021, 2020) with a radius of 250 m around the cave sites. **(c)** Pie chart showing the relative proportions of vegetation types as reported by authors. **(d)** Pie chart showing the relative proportions of land cover types as extracted from the Copernicus LCC database. Background shading in the map shows the global karst distribution extracted from the World Karst Aquifer Map (WoKAM; Goldscheider et al., 2020). To allow comparison between the two datasets, the Copernicus LCC vegetation data were grouped into broader categories, e.g. "deciduous" includes all closed and open broadleaf and needleleaf forest marked as deciduous. The entries in the database are more detailed.

The database contains both the original age model for individual entities and a standardized age-modelling ensemble. The original age model often takes account of site- and sample-specific conditions; the standardized age-model ensemble allows for robust assessment of age uncertainties and sensitivity testing (Comas-Bru et al., 2020). All codes for constructing the age-model ensembles using linear interpolation, linear regression, Bchron, Bacon, copRa, and StalAge can be found at https://github.com/paleovar/SISAL.AM (last access: 23 July 2020; Roesch and Rehfeld, 2020; codes licensed by the right holder(s) under a GPL-3). All age-model ensembles are available at https://doi.org/10.5281/zenodo.10726619 (Rehfeld and Büh-

ler, 2024). These codes are licensed by the right holder(s) under a Creative Commons Attribution 4.0 International licence.

The SISALv3 database, like its predecessors, lists the original references, and users are encouraged to consult original authors for interpretative details. The "SISAL webApp" (http://geochem.hu/SISAL_webApp; Hatvani et al., 2024) has been updated to provide an easy-to-use front-end interface for exploring the latest SISALv3 database. It now allows one to run queries on various data and metadata fields, such as stable isotope records and trace element proxies.

5.2 How to cite the database

The SISALv3 database is a community-driven effort to synthesize and standardize speleothem data and make them available to the wider palaeoclimate community. In agreement with the FAIR principles for scientific data management and stewardship, the database itself should be cited (available at https://doi.org/10.5287/ora-2nanwp4rk; Kaushal et al., 2024), along with this publication (and previous publication versions). If individual records are extracted from the database, the original publications should also be listed. More details on the terms of use are provided in the repository (https://doi.org/10.5287/ora-2nanwp4rk; Kaushal et al., 2024).

Supplement. The supplement related to this article is available online at: https://doi.org/10.5194/essd-16-1933-2024-supplement.

Team list. The following SISAL WG members contributed either data or age-modelling advice to SISALv3: Asfawossen Asrat (Department of Mining and Geological Engineering, Botswana International University of Science and Technology, Private Bag 16, Palapye, Botswana), Charlotte Honiat (Institute of Geology, University of Innsbruck, Innrain 52, Innsbruck, Austria), Dana Felicitas Christine Riechelmann (Institute for Geosciences, Johannes Gutenberg University of Mainz, Johann-Joachim-Becher-Weg 21, 55128 Mainz, Germany), Denis Scholz (Institute for Geosciences, Johannes Gutenberg University of Mainz, Johann-Joachim-Becher-Weg 21, 55128 Mainz, Germany), Dianbing Liu (School of Geography, Nanjing Normal University, Nanjing, China), Dominik Fleitmann (Department of Environmental Sciences, University of Basel, Bernoullistrasse 32, 4056 Basel, Switzerland), Dominik Hennhoefer (Department of Earth Sciences, Khalifa University, SAN Campus, Abu Dhabi, 127788, United Arab Emirates), Ezgi Ünal İmer (Geological Engineering Department, Middle East Technical University, 06800 Çankaya, Ankara, Türkiye), Gina E. Moseley (Institute of Geology, University of Innsbruck, Innrain 52, 6020 Innsbruck, Austria), Giselle Utida (Institute of Geosciences, University of São Paulo, São Paulo, 05508-080, Brazil), Hai Cheng (Institute of Global Environmental Change, Xi'an Jiaotong University, Xi'an, China), Helen Green (The University of Melbourne, Parkville, VIC 3010, Australia), Hsun-Ming Hu (High-Precision Mass Spectrometry and Environment Change Laboratory – HISPEC, Department of Geosciences, National Taiwan University, Taipei 10617, Taiwan), James Apaéstegui (Instituto Geofísico del Perú, Lima, 15012, Peru), Jan Esper (Department of Geography, Johannes Gutenberg University, Johann-Joachim-Becher-Weg 21, 55099 Mainz, Germany), Jasper A. Wassenburg (Center for Climate Physics, Institute for Basic Science, Busan, 46241, Republic of Korea; Pusan National University, Busan, 46241, Republic of Korea), Jeronimo Aviles Olguin (Museo del Desierto. Blvd. Carlos Abedrop Dávila 3745, Nuevo Centro Metropolitano de Saltillo, 25022 Saltillo, Coah. Mexico), Jessica Leigh Oster (Department of Earth and Environmental Sciences, Vanderbilt University, Nashville, TN 37240, USA), Jesús M. Pajón Morejón (National Museum of Natural History of Cuba, Department of Paleogeography and Paleobiology, Obispo 61, Plaza de Armas, Habana Vieja, CP 10 100, La Habana, Cuba), Judit Torner (CRG Marine Geosciences, Facultat de Ciències de la Terra, Universitat de Barcelona, 08028 Barcelona, Spain), Kathleen A Wendt (College of Earth, Ocean, and Atmospheric Sciences, Oregon State University, Corvallis, OR 97331, USA), Liangcheng Tan (State Key Laboratory of Loess and Quaternary Geology, Institute of Earth Environment, Chinese Academy of Sciences, Xi'an, China), Lijuan Sha (Institute of Global Environmental Change, Xi'an Jiaotong University, Xi'an, China), Liza Kathleen McDonough (ANSTO, New Illawarra Road, Lucas Heights, NSW 2234, Australia), Maša Surić (Department of Geography, University of Zadar, Ul. dr. F. Tuđmana 24 i, 23000 Zadar, Croatia), Matthew J. Jacobson (Division of Agrarian History, Department of Urban and Rural Development, Swedish University of Agricultural Sciences, 756 51 Uppsala, Sweden), Mercè Cisneros (GRC Geociències Marines, Departament de Dinàmica de la Terra i de l'Oceà, Facultat de Ciències de la Terra, Universitat de Barcelona, c/ Martí i Franqués s/n, 08028 Barcelona, Spain; Centre en Canvi Climàtic, Department de Geografia, Facultat de Turisme i Geografia, Universitat Rovira i Virgili, c/ Joanot Martorell 15, 43480 Vila-seca, Tarragona, Spain), Michael L. Griffiths (Department of Environmental Science, William Paterson University, Wayne, NJ 07739, USA), Michael Weber (Institute for Geosciences, Johannes Gutenberg University of Mainz, Johann-Joachim-Becher-Weg 21, 55128 Mainz, Germany), Nick Scroxton (Irish Climate and Analysis Research UnitS – ICARUS, Department of Geography, Maynooth University, Maynooth, Kildare, Ireland), Paul S. Wilcox (Institute of Geology, University of Innsbruck, Innrain 52, 6020 Innsbruck, Austria), R. Lawrence Edwards (Department of Earth and Environmental Sciences, University of Minnesota, Minneapolis, MN 55455, USA), Romina Belli (Proteomics and Mass Spectrometry Core Facility, Department of Cellular, Computational and Integrative Biology – DeCIBIO, University of Trento, Via Sommarive 9, 38123 Trento, Italy), Sebastian F. M. Breitenbach (Department of Geography and Environmental Sciences, Northumbria, Newcastle upon Tyne, NE1 8ST, UK), Shraddha T Band (National Taiwan University, Institute of Oceanography, National Taiwan University, No.1, Sec. 4, Roosevelt Road, Taipei 106, Taiwan), Simon Dominik Steidle (Institute of Geology, University of Innsbruck, Innrain 52, 6020 Innsbruck, Austria), Stacy Anne Carolin (Department of Earth Sciences, University of Cambridge, Downing Street, Cambridge, CB23 8AD, UK), Vanessa E. Johnston (Karst Research Institute ZRC SAZU, Titov trg 2, 6230 Postojna, Slovenia), and Wuhui Duan (Key Laboratory of Cenozoic Geology and Environment, Institute of Geology and Geophysics, Chinese Academy of Sciences, Beijing, China; CAS Center for Excellence in Life and Paleoenvironment, Beijing, China).

Author contributions. NK coordinated this project. NK, FAL, and MW designed the new version of the database. KR and JLB ran the SISAL standardized age–depth models for new entities. Downsampling of trace element records to stable isotope resolution was performed by VS and MR. Standardization of trace element data files was done by YB and NK. Reworking and additions to the metadata fields were done by KB and KA. JGS and NK collected citations, copyright information, and licence terms for the cave maps and speleothem images. Regional data collection and screening was coordinated by VA, JLB, SC, AC, LE, JH, IGH, ZK, AK, KK, MM,

BM, SMA, CN, VFN, CPM, JR, NaS, NiS, CVT, BHT, SW, AW, and HZ. Quality control of the submitted datasets was performed by MW, FAL, and NK, with additional code provided by JF. Figures 1 and 2 were created by FAL, and Figs. 3–9 were created by JCB. All authors listed as "Data contributors" provided data for this version of the database or helped to complete existing data entries. FL wrote the paper with input from NK, JCB, KR, AB, PT, and SPH. All authors contributed to the final version of the paper.

Competing interests. The contact author has declared that none of the authors has any competing interests.

Disclaimer. Publisher's note: Copernicus Publications remains neutral with regard to jurisdictional claims made in the text, published maps, institutional affiliations, or any other geographical representation in this paper. While Copernicus Publications makes every effort to include appropriate place names, the final responsibility lies with the authors.

Acknowledgements. We thank all SISAL members who contributed their data to this project and were available to provide additional information where necessary. We also acknowledge Ana Moreno, Christoph Spötl, and Laura A. Dupont for specific data contributions to the database. We thank the editorial staff at *Earth System Science Data*, the reviewers (Ewan Gowan, Christopher Hancock, and Sang Chen), and the anonymous referee for their supportive and critical feedback on this manuscript.

Financial support. This study was conducted by SISAL (Speleothem Isotopes Synthesis and Analysis), a working group of the Past Global Changes (PAGES) project. In this framework, we received financial support from the Swiss Academy of Sciences and the Chinese Academy of Sciences. The design and construction of the SISALv3 database were financially supported by a PAGES Data Stewardship Scholarship to Franziska A. Lechleitner and Nikita Kaushal (grant no. DSS-108). We also received funding from PAGES, the Minerva Stiftung (grant no. 3063000253), and the Institute of Earth Sciences at the Hebrew University Jerusalem (Israel) to support the organization of a workshop to kick-start the initiative.

Review statement. This paper was edited by Xingchen Wang and reviewed by Chris Hancock, Evan Gowan, Sang Chen, and one anonymous referee.

References

Allan, M., Deliège, A., Verheyden, S., Nicolay, S., Quinif, Y., and Fagel, N.: Evidence for solar influence in a Holocene speleothem record (Père Noël cave, SE Belgium), Quaternary Sci. Rev., 192, 249–262, https://doi.org/10.1016/j.quascirev.2018.05.039, 2018.

Andrews, J. E., Carolin, S. A., Peckover, E. N., Marca, A., Al-Omari, S., and Rowe, P. J.: Holocene stable isotope record of insolation and rapid climate change in a stalagmite from the Zagros of Iran, Quaternary Sci. Rev., 241, 106433, https://doi.org/10.1016/j.quascirev.2020.106433, 2020.

Apaéstegui, J., Cruz, F. W., Vuille, M., Fohlmeister, J., Espinoza, J. C., Sifeddine, A., Strikis, N., Guyot, J. L., Ventura, R., Cheng, H., and Edwards, R. L.: Precipitation changes over the eastern Bolivian Andes inferred from speleothem (δ18O) records for the last 1400 years, Earth Planet. Sc. Lett., 494, 124–134, https://doi.org/10.1016/j.epsl.2018.04.048, 2018.

Arienzo, M. M., Swart, P. K., Broad, K., Clement, A. C., Pourmand, A., and Kakuk, B.: Multi-proxy evidence of millennial climate variability from multiple Bahamian speleothems, Quaternary Sci. Rev., 161, 18–29, https://doi.org/10.1016/j.quascirev.2017.02.004, 2017.

Asrat, A., Baker, A., Leng, M. J., Hellstrom, J., Mariethoz, G., Boomer, I., Yu, D., Jex, C. N., and Gunn, J.: Paleoclimate change in Ethiopia around the last interglacial derived from annually-resolved stalagmite evidence, Quaternary Sci. Rev., 202, 197–210, https://doi.org/10.1016/j.quascirev.2018.06.016, 2018.

Atsawawaranunt, K., Comas-Bru, L., Amirnezhad Mozhdehi, S., Deininger, M., Harrison, S. P., Baker, A., Boyd, M., Kaushal, N., Ahmad, S. M., Ait Brahim, Y., Arienzo, M., Bajo, P., Braun, K., Burstyn, Y., Chawchai, S., Duan, W., Hatvani, I. G., Hu, J., Kern, Z., Labuhn, I., Lachniet, M., Lechleitner, F. A., Lorrey, A., Pérez-Mejías, C., Pickering, R., Scroxton, N., and SISAL Working Group Members: The SISAL database: a global resource to document oxygen and carbon isotope records from speleothems, Earth Syst. Sci. Data, 10, 1687–1713, https://doi.org/10.5194/essd-10-1687-2018, 2018.

Ayalon, A., Bar-Matthews, M., and Sass, E.: Rainfall-recharge relationships within a karstic terrain in the Eastern Mediterranean semi-arid region, Israel: δ^{18}O and δD characteristics, J. Hydrol., 207, 18–31, https://doi.org/10.1016/S0022-1694(98)00119-X, 1998.

Ayalon, A., Bar-Matthews, M., Frumkin, A., and Matthews, A.: Last Glacial warm events on Mount Hermon: the southern extension of the Alpine karst range of the east Mediterranean, Quaternary Sci. Rev., 59, 43–56, https://doi.org/10.1016/j.quascirev.2012.10.047, 2013.

Azevedo, V., Stríkis, N. M., Santos, R. A., de Souza, J. G., Ampuero, A., Cruz, F. W., de Oliveira, P., Iriarte, J., Stumpf, C. F., Vuille, M., Mendes, V. R., Cheng, H., and Edwards, R. L.: Medieval Climate Variability in the eastern Amazon-Cerrado regions and its archeological implications, Sci. Rep., 9, 20306, https://doi.org/10.1038/s41598-019-56852-7, 2019.

Azevedo, V., Strikis, N. M., Novello, V. F., Roland, C. L., Cruz, F. W., Santos, R. V., Vuille, M., Utida, G., De Andrade, F. R. D., Cheng, H., and Edwards, R. L.: Paleovegetation seesaw in Brazil since the Late Pleistocene: A multiproxy study of two biomes, Earth Planet. Sc. Lett., 563, 116880, https://doi.org/10.1016/j.epsl.2021.116880, 2021.

Badertscher, S., Fleitmann, D., Cheng, H., Edwards, R. L., Göktürk, O. M., Zumbühl, A., Leuenberger, M., and Tüysüz, O.: Pleistocene water intrusions from the Mediterranean and Caspian seas into the Black Sea, Nat. Geosci., 4, 236–239, https://doi.org/10.1038/ngeo1106, 2011.

Baker, A., Ito, E., Smart, P. L., and McEwan, R. F.: Elevated and variable values of ^{13}C in speleothems in a British cave sys-

tem, Chem. Geol., 136, 263–270, https://doi.org/10.1016/S0009-2541(96)00129-5, 1997.

Baker, A., Hartmann, A., Duan, W., Hankin, S., Comas-Bru, L., Cuthbert, M. O., Treble, P. C., Banner, J., Genty, D., Baldini, L. M., Bartolomé, M., Moreno, A., Pérez-Mejías, C., and Werner, M.: Global analysis reveals climatic controls on the oxygen isotope composition of cave drip water, Nat. Commun., 10, 2984, https://doi.org/10.1038/s41467-019-11027-w, 2019.

Baker, A., Mariethoz, G., Comas-Bru, L., Hartmann, A., Frisia, S., Borsato, A., Treble, P. C., and Asrat, A.: The Properties of Annually Laminated Stalagmites-A Global Synthesis, Rev. Geophys., 59, e2020RG000722, https://doi.org/10.1029/2020RG000722, 2021.

Baldini, J. U. L., Lechleitner, F. A., Breitenbach, S. F. M., Van Hunen, J., Baldini, L. M., Wynn, P. M., Jamieson, R. A., Ridley, H. E., Baker, A. J., Walczak, I. W., and Fohlmeister, J.: Detecting and quantifying palaeoseasonality in stalagmites using geochemical and modelling approaches, Quaternary Sci. Rev., 254, 106784, https://doi.org/10.1016/j.quascirev.2020.106784, 2021.

Baldini, L. M., Baldini, J. U. L., McDermott, F., Arias, P., Cueto, M., Fairchild, I. J., Hoffmann, D. L., Mattey, D. P., Müller, W., Nita, D. C., Ontañón, R., Garciá-Moncó, C., and Richards, D. A.: North Iberian temperature and rainfall seasonality over the Younger Dryas and Holocene, Quaternary Sci. Rev., 226, 105998, https://doi.org/10.1016/j.quascirev.2019.105998, 2019.

Band, S. T., Yadava, M. G., Kaushal, N., Midhun, M., Thirumalai, K., Francis, T., Laskar, A., Ramesh, R., Henderson, G. M., and Narayana, A. C.: Southern hemisphere forced millennial scale Indian summer monsoon variability during the late Pleistocene, Sci. Rep., 12, 10136, https://doi.org/10.1038/s41598-022-14010-6, 2022.

Bar-Matthews, M., Ayalon, A., Gilmour, M., Matthews, A., and Hawkesworth, C. J.: Sea-land oxygen isotopic relationships from planktonic foraminifera and speleothems in the Eastern Mediterranean region and their implication for paleorainfall during interglacial intervals, Geochim. Cosmochim. Ac., 67, 3181–3199, https://doi.org/10.1016/S0016-7037(02)01031-1, 2003.

Bar-Matthews, M., Marean, C. W., Jacobs, Z., Karkanas, P., Fisher, E. C., Herries, A. I. R., Brown, K., Williams, H. M., Bernatchez, J., Ayalon, A., and Nilssen, P. J.: A high resolution and continuous isotopic speleothem record of paleoclimate and paleoenvironment from 90 to 53 ka from Pinnacle Point on the south coast of South Africa, Quaternary Sci. Rev., 29, 2131–2145, https://doi.org/10.1016/j.quascirev.2010.05.009, 2010.

Belli, R., Frisia, S., Borsato, A., Drysdale, R., Hellstrom, J., Zhao, J. X., and Spötl, C.: Regional climate variability and ecosystem responses to the last deglaciation in the northern hemisphere from stable isotope data and calcite fabrics in two northern Adriatic stalagmites, Quaternary Sci. Rev., 72, 146–158, https://doi.org/10.1016/j.quascirev.2013.04.014, 2013.

Belli, R., Borsato, A., Frisia, S., Drysdale, R., Maas, R., and Greig, A.: Investigating the hydrological significance of stalagmite geochemistry (Mg, Sr) using Sr isotope and particulate element records across the Late Glacial-to-Holocene transition, Geochim. Cosmochim. Ac., 199, 247–263, https://doi.org/10.1016/j.gca.2016.10.024, 2017.

Bernal-Wormull, J. L., Moreno, A., Pérez-Mejías, C., Bartolomé, M., Aranburu, A., Arriolabengoa, M., Iriarte, E., Cacho, I., Spötl, C., Edwards, R. L., and Cheng, H.: Immediate temperature response in northern Iberia to last deglacial changes in the North Atlantic, Geology, 49, 999–1003, https://doi.org/10.1130/G48660.1, 2021.

Borsato, A., Frisia, S., Fairchild, I. J., Somogyi, A., and Susini, J.: Trace element distribution in annual stalagmite laminae mapped by micrometer-resolution X-ray fluorescence: Implications for incorporation of environmentally significant species, Geochim. Cosmochim. Ac., 71, 1494–1512, https://doi.org/10.1016/j.gca.2006.12.016, 2007.

Braun, K., Bar-Matthews, M., Matthews, A., Ayalon, A., Cowling, R. M., Karkanas, P., Fisher, E. C., Dyez, K., Zilberman, T., and Marean, C. W.: Late Pleistocene records of speleothem stable isotopic compositions from Pinnacle Point on the South African south coast, Quaternary Res., 91, 265–288, https://doi.org/10.1017/qua.2018.61, 2019a.

Braun, K., Nehme, C., Pickering, R., Rogerson, M., and Scroxton, N.: A Window into Africa's Past Hydroclimates: The SISAL_v1 Database Contribution, Quaternary, 2, 4, https://doi.org/10.3390/quat2010004, 2019b.

Braun, K., Bar-Matthews, M., Matthews, A., Ayalon, A., Zilberman, T., Cowling, R. M., Fisher, E. C., Herries, A. I. R., Brink, J. S., and Marean, C. W.: Comparison of climate and environment on the edge of the Palaeo-Agulhas Plain to the Little Karoo (South Africa) in Marine Isotope Stages 5–3 as indicated by speleothems, Quaternary Sci. Rev., 235, 105803, https://doi.org/10.1016/j.quascirev.2019.06.025, 2020.

Buchhorn, M., Lesiv, M., Tsendbazar, N.-E., Herold, M., Bertels, L., and Smets, B.: Copernicus Global Land Cover Layers – Collection 2, Remote Sensing, 12, 1044, https://doi.org/10.3390/rs12061044, 2020.

Buchhorn, M., Smets, B., Bertels, L., Roo, B. D., Lesiv, M., Tsendbazar, N.-E., Li, L., and Tarko, A.: Copernicus Global Land Service: Land Cover 100m: version 3 Globe 2015–2019: Product User Manual, Zenodo [manual], https://doi.org/10.5281/zenodo.4723921, 2021.

Buckingham, F. L., Carolin, S. A., Partin, J. W., Adkins, J. F., Cobb, K. M., Day, C. C., Ding, Q., He, C., Liu, Z., Otto-Bliesner, B., Roberts, W. H. G., Lejau, S., and Malang, J.: Termination 1 Millennial-Scale Rainfall Events Over the Sunda Shelf, Geophys. Res. Lett., 49, e2021GL096937, https://doi.org/10.1029/2021GL096937, 2022.

Budsky, A., Scholz, D., Wassenburg, J. A., Mertz-Kraus, R., Spötl, C., Riechelmann, D. F., Gibert, L., Jochum, K. P., and Andreae, M. O.: Speleothem δ^{13} C record suggests enhanced spring/summer drought in south-eastern Spain between 9.7 and 7.8 ka – A circum-Western Mediterranean anomaly?, The Holocene, 29, 1113–1133, https://doi.org/10.1177/0959683619838021, 2019.

Bühler, J. C., Axelsson, J., Lechleitner, F. A., Fohlmeister, J., LeGrande, A. N., Midhun, M., Sjolte, J., Werner, M., Yoshimura, K., and Rehfeld, K.: Investigating stable oxygen and carbon isotopic variability in speleothem records over the last millennium using multiple isotope-enabled climate models, Clim. Past, 18, 1625–1654, https://doi.org/10.5194/cp-18-1625-2022, 2022.

Burstyn, Y., Martrat, B., Lopez, J. F., Iriarte, E., Jacobson, M. J., Lone, M. A., and Deininger, M.: Speleothems from the Middle East: An Example of Water Limited Environments in the SISAL Database, Quaternary, 2, 16, https://doi.org/10.3390/quat2020016, 2019.

Carolin, S. A., Ersek, V., Roberts, W. H. G., Walker, R. T., and Henderson, G. M.: Drying in the Middle East During Northern Hemisphere Cold Events of the Early Glacial Period, Geophys. Res. Lett., 46, 14003–14010, https://doi.org/10.1029/2019GL084365, 2019a.

Carolin, S. A., Walker, R. T., Day, C. C., Ersek, V., Sloan, R. A., Dee, M. W., Talebian, M., and Henderson, G. M.: Precise timing of abrupt increase in dust activity in the Middle East coincident with 4.2 ka social change, P. Natl. Acad. Sci. USA, 116, 67–72, https://doi.org/10.1073/pnas.1808103115, 2019b.

Chawchai, S., Tan, L., Löwemark, L., Wang, H.-C., Yu, T.-L., Chung, Y.-C., Mii, H.-S., Liu, G., Blaauw, M., Gong, S.-Y., Wohlfarth, B., and Shen, C.-C.: Hydroclimate variability of central Indo-Pacific region during the Holocene, Quaternary Sci. Rev., 253, 106779, https://doi.org/10.1016/j.quascirev.2020.106779, 2021.

Chen, C., Yuan, D., Cheng, H., Yu, T., Shen, C., Edwards, R. L., Wu, Y., Xiao, S., Zhang, J., Wang, T., Huang, R., Liu, Z., Li, T., and Li, J.: Human activity and climate change triggered the expansion of rocky desertification in the karst areas of Southwestern China, Sci. China Earth Sci., 64, 1761–1773, https://doi.org/10.1007/s11430-020-9760-7, 2021.

Cheng, H., Edwards, R. L., Broecker, W. S., Denton, G. H., Kong, X., Wang, Y., Zhang, R., and Wang, X.: Ice age terminations., Science (New York, N.Y.), 326, 248–252, https://doi.org/10.1126/science.1177840, 2009a.

Cheng, H., Fleitmann, D., Edwards, R. L., Wang, X., Cruz, F. W., Auler, A. S., Mangini, A., Wang, Y., Kong, X., Burns, S. J., and Matter, A.: Timing and structure of the 8.2 kyr B.P. event inferred from δ^{18}O records of stalagmites from China, Oman, and Brazil, Geology, 37, 1007–1010, https://doi.org/10.1130/G30126A.1, 2009b.

Cheng, H., Sinha, A., Cruz, F. W., Wang, X., Edwards, R. L., Horta, F. M., Ribas, C. C., Vuille, M., Stott, L. D., and Auler, A. S.: Climate change in Amazonia and biodiversity, Nat. Commun., 4, 1411, https://doi.org/10.1038/ncomms2415, 2013.

Cheng, H., Edwards, R. L., Sinha, A., Spötl, C., Yi, L., Chen, S., Kelly, M., Kathayat, G., Wang, X., Li, X., Kong, X., Wang, Y., Ning, Y., and Zhang, H.: The Asian monsoon over the past 640,000 years and ice age terminations, Nature, 534, 640–646, https://doi.org/10.1038/nature18591, 2016.

Cheng, H., Springer, G. S., Sinha, A., Hardt, B. F., Yi, L., Li, H., Tian, Y., Li, X., Rowe, H. D., Kathayat, G., Ning, Y., and Edwards, R. L.: Eastern North American climate in phase with fall insolation throughout the last three glacial-interglacial cycles, Earth Planet. Sc. Lett., 522, 125–134, https://doi.org/10.1016/j.epsl.2019.06.029, 2019.

Cheng, H., Xu, Y., Dong, X., Zhao, J., Li, H., Baker, J., Sinha, A., Spötl, C., Zhang, H., Du, W., Zong, B., Jia, X., Kathayat, G., Liu, D., Cai, Y., Wang, X., Strikis, N. M., Cruz, F. W., Auler, A. S., Gupta, A. K., Singh, R. K., Jaglan, S., Dutt, S., Liu, Z., and Edwards, R. L.: Onset and termination of Heinrich Stadial 4 and the underlying climate dynamics, Commun. Earth Environ., 2, 1–11, https://doi.org/10.1038/s43247-021-00304-6, 2021.

Cisneros, M., Cacho, I., Moreno, A., Stoll, H., Torner, J., Català, A., Edwards, R. L., Cheng, H., and Fornós, J. J.: Hydroclimate variability during the last 2700 years based on stalagmite multi-proxy records in the central-western Mediterranean, Quaternary Sci. Rev., 269, 107137, https://doi.org/10.1016/j.quascirev.2021.107137, 2021.

Columbu, A., Drysdale, R., Hellstrom, J., Woodhead, J., Cheng, H., Hua, Q., Zhao, J., Montagna, P., Pons-Branchu, E., and Edwards, R. L.: U-Th and radiocarbon dating of calcite speleothems from gypsum caves (Emilia Romagna, North Italy), Quaternary Geochron., 52, 51–62, https://doi.org/10.1016/j.quageo.2019.04.002, 2019.

Columbu, A., Chiarini, V., Spötl, C., Benazzi, S., Hellstrom, J., Cheng, H., and De Waele, J.: Speleothem record attests to stable environmental conditions during Neanderthal–modern human turnover in southern Italy, Nat. Ecol. Evol., 4, 1188–1195, https://doi.org/10.1038/s41559-020-1243-1, 2020.

Columbu, A., Spötl, C., Fohlmeister, J., Hu, H.-M., Chiarini, V., Hellstrom, J., Cheng, H., Shen, C.-C., and De Waele, J.: Central Mediterranean rainfall varied with high northern latitude temperatures during the last deglaciation, Commun. Earth Environ., 3, 1–9, https://doi.org/10.1038/s43247-022-00509-3, 2022.

Comas-Bru, L. and Harrison, S. P.: SISAL: Bringing added value to speleothem research, Quaternary, 2, 7, https://doi.org/10.3390/quat2010007, 2019.

Comas-Bru, L., Deininger, M., Harrison, S., Bar-Matthews, M., Baker, A., Duan, W., and Stríkis, N.: Speleothem synthesis and analysis working group, PAGES Mag., 25, 129–129, https://doi.org/10.22498/pages.25.2.129, 2017.

Comas-Bru, L., Harrison, S. P., Werner, M., Rehfeld, K., Scroxton, N., Veiga-Pires, C., and SISAL working group members: Evaluating model outputs using integrated global speleothem records of climate change since the last glacial, Clim. Past, 15, 1557–1579, https://doi.org/10.5194/cp-15-1557-2019, 2019.

Comas-Bru, L., Rehfeld, K., Roesch, C., Amirnezhad-Mozhdehi, S., Harrison, S. P., Atsawawaranunt, K., Ahmad, S. M., Brahim, Y. A., Baker, A., Bosomworth, M., Breitenbach, S. F. M., Burstyn, Y., Columbu, A., Deininger, M., Demény, A., Dixon, B., Fohlmeister, J., Hatvani, I. G., Hu, J., Kaushal, N., Kern, Z., Labuhn, I., Lechleitner, F. A., Lorrey, A., Martrat, B., Novello, V. F., Oster, J., Pérez-Mejías, C., Scholz, D., Scroxton, N., Sinha, N., Ward, B. M., Warken, S., Zhang, H., and SISAL Working Group members: SISALv2: a comprehensive speleothem isotope database with multiple age–depth models, Earth Syst. Sci. Data, 12, 2579–2606, https://doi.org/10.5194/essd-12-2579-2020, 2020.

Covington, M. D. and Perne, M.: Consider a cylindrical cave: A physicist's view of cave and karst science, Acta Carsologica, 44, 363–380, https://doi.org/10.3986/ac.v44i3.1925, 2015.

Cruz, F. W., Burns, S. J., Jercinovic, M., Karmann, I., Sharp, W. D., and Vuille, M.: Evidence of rainfall variations in Southern Brazil from trace element ratios (Mg/Ca and Sr/Ca) in a Late Pleistocene stalagmite, Geochim. Cosmochim. Ac., 71, 2250–2263, https://doi.org/10.1016/j.gca.2007.02.005, 2007.

Day, C. C. and Henderson, G. M.: Controls on trace-element partitioning in cave-analogue calcite, Geochim. Cosmochim. Ac., 120, 612–627, https://doi.org/10.1016/j.gca.2013.05.044, 2013.

Deininger, M., Ward, B. M., Novello, V. F., and Cruz, F. W.: Late Quaternary Variations in the South American Monsoon System as Inferred by Speleothems—New Perspectives Using the SISAL Database, Quaternary, 2, 6, https://doi.org/10.3390/quat2010006, 2019.

Della Libera, M. E., Novello, V. F., Cruz, F. W., Orrison, R., Vuille, M., Maezumi, S. Y., de Souza, J., Cauhy, J., Campos, J. L. P. S., Ampuero, A., Utida, G., Stríkis, N. M., Stumpf, C. F., Azevedo, V., Zhang, H., Edwards, R. L., and Cheng, H.: Paleoclimatic and paleoenvironmental changes in Amazonian lowlands over the last three millennia, Quaternary Sci. Rev., 279, 107383, https://doi.org/10.1016/j.quascirev.2022.107383, 2022.

Dorale, J. A., Edwards, L. R., Ito, E., and Gonzalez, L. A.: Climate and Vegetation History of the Midcontinent from 75 to 25 ka: A Speleothem Record from Crevice Cave, Missouri, USA | Science, Science (New York, N.Y.), 282, 1871–1874, 1998.

Drysdale, R., Couchoud, I., Zanchetta, G., Isola, I., Regattieri, E., Hellstrom, J., Govin, A., Tzedakis, P. C., Ireland, T., Corrick, E., Greig, A., Wong, H., Piccini, L., Holden, P., and Woodhead, J.: Magnesium in subaqueous speleothems as a potential palaeotemperature proxy, Nat. Commun., 11, 5027, https://doi.org/10.1038/s41467-020-18083-7, 2020.

Duan, W., Cheng, H., Tan, M., Li, X., and Lawrence Edwards, R.: Timing and structure of Termination II in north China constrained by a precisely dated stalagmite record, Earth Planet. Sc. Lett., 512, 1–7, https://doi.org/10.1016/j.epsl.2019.01.043, 2019.

Duan, W., Wang, X., Tan, M., Cui, L., Wang, X., and Xiao, Z.: Variable Phase Relationship Between Monsoon and Temperature in East Asia During Termination II Revealed by Oxygen and Clumped Isotopes of a Northern Chinese Stalagmite, Geophys. Res. Lett., 49, e2022GL098296, https://doi.org/10.1029/2022GL098296, 2022.

Dupont, L. A., Railsback, L. B., Liang, F., Brook, G. A., Cheng, H., and Edwards, R. L.: Episodic deposition of stalagmites in the northeastern Democratic Republic of the Congo suggests Equatorial Humid Periods during insolation maxima, Quaternary Sci. Rev., 286, 107552, https://doi.org/10.1016/j.quascirev.2022.107552, 2022.

Fairchild, I. J. and Treble, P. C.: Trace elements in speleothems as recorders of environmental change, Quaternary Sci. Rev., 28, 449–468, https://doi.org/10.1016/j.quascirev.2008.11.007, 2009.

Fairchild, I. J., Borsato, A., Tooth, A. F., Frisia, S., Hawkesworth, C. J., Huang, Y., McDermott, F., and Spiro, B.: Controls on trace element (Sr-Mg) compositions of carbonate cave waters: implications for speleothem climatic records, Chem. Geol., 166, 255–269, 2000.

Faraji, M., Borsato, A., Frisia, S., Hartland, A., Hellstrom, J. C., and Greig, A.: High-resolution reconstruction of infiltration in the Southern Cook Islands based on trace elements in speleothems, Quaternary Res., 118, 1–21, https://doi.org/10.1017/qua.2023.51, 2023.

Finestone, E. M., Breeze, P. S., Breitenbach, S. F. M., Drake, N., Bergmann, L., Maksudov, F., Muhammadiyev, A., Scott, P., Cai, Y., Khatsenovich, A. M., Rybin, E. P., Nehrke, G., Boivin, N., and Petraglia, M.: Paleolithic occupation of arid Central Asia in the Middle Pleistocene, PLOS ONE, 17, e0273984, https://doi.org/10.1371/journal.pone.0273984, 2022.

Flohr, P., Fleitmann, D., Zorita, E., Sadekov, A., Cheng, H., Bosomworth, M., Edwards, L., Matthews, W., and Matthews, R.: Late Holocene droughts in the Fertile Crescent recorded in a speleothem from northern Iraq, Geophys. Res. Lett., 44, 1528–1536, https://doi.org/10.1002/2016GL071786, 2017.

Fohlmeister, J., Vollweiler, N., Spötl, C., and Mangini, A.: COMNISPA II: Update of a mid-European isotope climate record, 11 ka to present, The Holocene, 23, 749–754, https://doi.org/10.1177/0959683612465446, 2013.

Fohlmeister, J., Voarintsoa, N. R. G., Lechleitner, F. A., Boyd, M., Brandtstätter, S., Jacobson, M. J., and Oster, J. L.: Main controls on the stable carbon isotope composition of speleothems, Geochim. Cosmochim. Ac., 279, 67–87, https://doi.org/10.1016/j.gca.2020.03.042, 2020.

Frumkin, A., Ford, D. C., and Schwarcz, H. P.: Continental Oxygen Isotopic Record of the Last 170,000 Years in Jerusalem, Quaternary Res., 51, 317–327, https://doi.org/10.1006/qres.1998.2031, 1999.

Genty, D., Blamart, D., Ouahdi, R., Gilmour, M., Baker, A., Jouzel, J., and Van-Exter, S.: Precise dating of Dansgaard-Oeschger climate oscillations in western Europe from stalagmite data, Nature, 421, 833–837, https://doi.org/10.1038/nature01391, 2003.

Genty, D., Blamart, D., Ghaleb, B., Plagnes, V., Causse, C., Bakalowicz, M., Zouari, K., Chkir, N., Hellstrom, J., Wainer, K., and Bourges, F.: Timing and dynamics of the last deglaciation from European and North African $\delta^{13}C$ stalagmite profiles – Comparison with Chinese and South Hemisphere stalagmites, Quaternary Sci. Rev., 25, 2118–2142, https://doi.org/10.1016/j.quascirev.2006.01.030, 2006.

Goede, A., McCulloch, M., McDermott, F., and Hawkesworth, C.: Aeolian contribution to strontium and strontium isotope variations in a tasmanian speleothem, Chem. Geol., 149, 37–50, https://doi.org/10.1016/S0009-2541(98)00035-7, 1998.

Goldscheider, N., Chen, Z., Auler, A. S., Bakalowicz, M., Broda, S., Drew, D., Hartmann, J., Jiang, G., Moosdorf, N., Stevanovic, Z., and Veni, G.: Global distribution of carbonate rocks and karst water resources, Hydrogeol. J., 28, 1661–1677, https://doi.org/10.1007/s10040-020-02139-5, 2020.

Green, H., Pickering, R., Drysdale, R., Johnson, B. C., Hellstrom, J., and Wallace, M.: Evidence for global teleconnections in a late Pleistocene speleothem record of water balance and vegetation change at Sudwala Cave, South Africa, Quaternary Sci. Rev., 110, 114–130, https://doi.org/10.1016/j.quascirev.2014.11.016, 2015.

Griffiths, M. L., Johnson, K. R., Pausata, F. S. R., White, J. C., Henderson, G. M., Wood, C. T., Yang, H., Ersek, V., Conrad, C., and Sekhon, N.: End of Green Sahara amplified mid- to late Holocene megadroughts in mainland Southeast Asia, Nat. Commun., 11, 4204, https://doi.org/10.1038/s41467-020-17927-6, 2020.

Hatvani, I. G., Kern, Z., Tanos, P., Wilhelm, M., Lechleitner, F. A., and Kaushal, N.: The SISAL webApp: exploring the speleothem climate and environmental archives of the world, Quaternary Res., 118, 1–7, https://doi.org/10.1017/qua.2023.39, 2024 (data available at: http://geochem.hu/SISAL_webApp, last access: 8 March 2024).

Henderson, G. M.: Caving in to new chronologies., Science, 313, 620–622, https://doi.org/10.1126/science.1128980, 2006.

Honiat, C., Festi, D., Wilcox, P. S., Edwards, R. L., Cheng, H., and Spötl, C.: Early Last Interglacial environmental changes recorded by speleothems from Katerloch (south-east Austria), J. Quaternary Sci., 37, 664–676, https://doi.org/10.1002/jqs.3398, 2022.

Hu, C., Henderson, G. M., Huang, J., Xie, S., Sun, Y., and Johnson, K. R.: Quantification of Holocene Asian monsoon rainfall from spatially separated cave records, Earth Planet. Sc. Lett., 266, 221–232, https://doi.org/10.1016/j.epsl.2007.10.015, 2008.

Hu, H.-M., Michel, V., Valensi, P., Mii, H.-S., Starnini, E., Zunino, M., and Shen, C.-C.: Stalagmite-Inferred Climate in the Western Mediterranean during the Roman Warm Period, Climate, 10, 93, https://doi.org/10.3390/cli10070093, 2022.

Huang, Y., Fairchild, I. J., Borsato, A., Frisia, S., Cassidy, N. J., McDermott, F., and Hawkesworth, C. J.: Seasonal variations in Sr, Mg and P in modern speleothems (Grotta di Ernesto, Italy), Chem. Geol., 175, 429–448, https://doi.org/10.1016/S0009-2541(00)00337-5, 2001.

Jacobson, M. J., Flohr, P., Gascoigne, A., Leng, M. J., Sadekov, A., Cheng, H., Edwards, R. L., Tüysüz, O., and Fleitmann, D.: Heterogenous Late Holocene Climate in the Eastern Mediterranean – The Kocain Cave Record From SW Turkey, Geophys. Res. Lett., 48, e2021GL094733, https://doi.org/10.1029/2021GL094733, 2021.

Jamieson, R. A., Baldini, J. U. L., Brett, M. J., Taylor, J., Ridley, H. E., Ottley, C. J., Prufer, K. M., Wassenburg, J. A., Scholz, D., and Breitenbach, S. F. M.: Intra- and inter-annual uranium concentration variability in a Belizean stalagmite controlled by prior aragonite precipitation: A new tool for reconstructing hydro-climate using aragonitic speleothems, Geochim. Cosmochim. Ac., 190, 332–346, https://doi.org/10.1016/j.gca.2016.06.037, 2016.

Jochum, K. P., Scholz, D., Stoll, B., Weis, U., Wilson, S. A., Yang, Q., Schwalb, A., Börner, N., Jacob, D. E., and Andreae, M. O.: Accurate trace element analysis of speleothems and biogenic calcium carbonates by LA-ICP-MS, Chem. Geol., 318–319, 31–44, https://doi.org/10.1016/j.chemgeo.2012.05.009, 2012.

Johnson, K. R., Hu, C., Belshaw, N. S., and Henderson, G. M.: Seasonal trace-element and stable-isotope variations in a Chinese speleothem: The potential for high-resolution paleomonsoon reconstruction, Earth Planet. Sc. Lett., 244, 394–407, https://doi.org/10.1016/j.epsl.2006.01.064, 2006.

Johnston, V. E., Borsato, A., Frisia, S., Spötl, C., Hellstrom, J. C., Cheng, H., and Edwards, R. L.: Last interglacial hydroclimate in the Italian Prealps reconstructed from speleothem multi-proxy records (Bigonda Cave, NE Italy), Quaternary Sci. Rev., 272, 107243, https://doi.org/10.1016/j.quascirev.2021.107243, 2021.

Kathayat, G., Cheng, H., Sinha, A., Spötl, C., Edwards, R. L., Zhang, H., Li, X., Yi, L., Ning, Y., Cai, Y., Lui Lui, W., and Breitenbach, S. F. M.: Indian monsoon variability on millennial-orbital timescales, Sci. Rep., 6, 24374, https://doi.org/10.1038/srep24374, 2016.

Kaushal, N., Breitenbach, S. F. M., Lechleitner, F. A., Sinha, A., Tewari, V. C., Ahmad, S. M., Berkelhammer, M., Band, S., Yadava, M., Ramesh, R., and Henderson, G. M.: The Indian Summer Monsoon from a Speleothem δ18O Perspective – A Review, Quaternary, 1, 29, https://doi.org/10.3390/quat1030029, 2018.

Kaushal, N., Lechleitner, F. A., Wilhelm, M., and SISAL Working Group members: SISALv3: Speleothem Isotopes Synthesis and AnaLysis Database Version 3.0, University of Oxford [data set], https://doi.org/10.5287/ora-2nanwp4rk, 2024.

Kelly, M. J., Edwards, R. L., Cheng, H., Yuan, D., Cai, Y., Zhang, M., Lin, Y., and An, Z.: High resolution characterization of the Asian Monsoon between 146,000 and 99,000 years B.P. from Dongge Cave, China and global correlation of events surrounding Termination II, Palaeogeogr. Palaeocl., 236, 20–38, https://doi.org/10.1016/j.palaeo.2005.11.042, 2006.

Kern, Z., Demény, A., Perşoiu, A., and Hatvani, I. G.: Speleothem Records from the Eastern Part of Europe and Turkey – Discussion on Stable Oxygen and Carbon Isotopes, Quaternary, 2, 31, https://doi.org/10.3390/quat2030031, 2019.

Koltai, G., Spötl, C., Shen, C.-C., Wu, C.-C., Rao, Z., Palcsu, L., Kele, S., Surányi, G., and Bárány-Kevei, I.: A penultimate glacial climate record from southern Hungary, J. Quaternary Sci., 32, 946–956, https://doi.org/10.1002/jqs.2968, 2017.

Lachniet, M. S., Denniston, R. F., Asmerom, Y., and Polyak, V. J.: Orbital control of western North America atmospheric circulation and climate over two glacial cycles, Nat. Commun., 5, 3805, https://doi.org/10.1038/ncomms4805, 2014.

Lechleitner, F. A., Amirnezhad-Mozhdehi, S., Columbu, A., Comas-Bru, L., Labuhn, I., Pérez-Mejías, C., and Rehfeld, K.: The Potential of Speleothems from Western Europe as Recorders of Regional Climate: A Critical Assessment of the SISAL Database, Quaternary, 1, 30, https://doi.org/10.3390/quat1030030, 2018.

Lechleitner, F. A., Day, C. C., Kost, O., Wilhelm, M., Haghipour, N., Henderson, G. M., and Stoll, H. M.: Stalagmite carbon isotopes suggest deglacial increase in soil respiration in western Europe driven by temperature change, Clim. Past, 17, 1903–1918, https://doi.org/10.5194/cp-17-1903-2021, 2021.

Li, H., Sinha, A., Anquetil André, A., Spötl, C., Vonhof, H. B., Meunier, A., Kathayat, G., Duan, P., Voarintsoa, N. R. G., Ning, Y., Biswas, J., Hu, P., Li, X., Sha, L., Zhao, J., Edwards, R. L., and Cheng, H.: A multimillennial climatic context for the megafaunal extinctions in Madagascar and Mascarene Islands, Sci. Adv., 6, eabb2459, https://doi.org/10.1126/sciadv.abb2459, 2020.

Li, H., Spötl, C., and Cheng, H.: A high-resolution speleothem proxy record of the Late Glacial in the European Alps: extending the NALPS19 record until the beginning of the Holocene, J. Quaternary Sci., 36, 29–39, https://doi.org/10.1002/jqs.3255, 2021.

Li, H.-C., Ku, T.-L., You, C.-F., Cheng, H., Edwards, R. L., Ma, Z.-B., Tsai, W., and Li, M.-D.: 87Sr/86Sr and Sr/Ca in speleothems for paleoclimate reconstruction in Central China between 70 and 280 kyr ago, Geochim. Cosmochim. Ac., 69, 3933–3947, https://doi.org/10.1016/j.gca.2005.01.009, 2005.

Li, T.-Y., Baker, J. L., Wang, T., Zhang, J., Wu, Y., Li, H.-C., Blyakharchuk, T., Yu, T.-L., Shen, C.-C., Cheng, H., Kong, X.-G., Xie, W.-L., and Edwards, R. L.: Early Holocene permafrost retreat in West Siberia amplified by reorganization of westerly wind systems, Commun. Earth Environ., 2, 1–11, https://doi.org/10.1038/s43247-021-00238-z, 2021.

Liu, D., Wang, Y., Cheng, H., Edwards, R. L., Kong, X., Chen, S., and Liu, S.: Contrasting Patterns in Abrupt Asian Summer Monsoon Changes in the Last Glacial Period and the Holocene, Paleoceanogr. Paleocl., 33, 214–226, https://doi.org/10.1002/2017PA003294, 2018.

Liu, D., Mi, X., Liu, S., and Wang, Y.: Multi-phased Asian hydroclimate variability during Heinrich Stadial 5, Clim. Dynam., 60, 4003–4016, https://doi.org/10.1007/s00382-022-06566-w, 2023.

Liu, G., Li, X., Chiang, H.-W., Cheng, H., Yuan, S., Chawchai, S., He, S., Lu, Y., Aung, L. T., Maung, P. M., Tun, W. N., Oo, K. M., and Wang, X.: On the glacial-interglacial variability of the Asian monsoon in speleothem δ^{18}O records, Sci. Adv., 6, eaay8189, https://doi.org/10.1126/sciadv.aay8189, 2020.

Lorrey, A. M., Williams, P. W., Woolley, J.-M., Fauchereau, N. C., Hartland, A., Bostock, H., Eaves, S., Lachniet, M. S., Renwick, J. A., and Varma, V.: Late Quaternary Climate Vari-

ability and Change from Aotearoa New Zealand Speleothems: Progress in Age Modelling, Oxygen Isotope Master Record Construction and Proxy-Model Comparisons, Quaternary, 3, 24, https://doi.org/10.3390/quat3030024, 2020.

Luetscher, M., Moseley, G. E., Festi, D., Hof, F., Edwards, R. L., and Spötl, C.: A Last Interglacial speleothem record from the Sieben Hengste cave system (Switzerland): Implications for alpine paleovegetation, Quaternary Sci. Rev., 262, 106974, https://doi.org/10.1016/j.quascirev.2021.106974, 2021.

Magiera, M., Lechleitner, F. A., Erhardt, A. M., Hartland, A., Kwiecien, O., Cheng, H., Bradbury, H. J., Turchyn, A. V., Riechelmann, S., Edwards, L., and Breitenbach, S. F. M.: Local and Regional Indian Summer Monsoon Precipitation Dynamics During Termination II and the Last Interglacial, Geophys. Res. Lett., 46, 12454–12463, https://doi.org/10.1029/2019GL083721, 2019.

Mangini, A., Spötl, C., and Verdes, P.: Reconstruction of temperature in the Central Alps during the past 2000 yr from a d18O stalagmite record, Earth Planet. Sc. Lett., 235, 741–751, https://doi.org/10.1016/j.epsl.2005.05.010, 2005.

Markowska, M., Cuthbert, M. O., Baker, A., Treble, P. C., Andersen, M. S., Adler, L., Griffiths, A., and Frisia, S.: Modern speleothem oxygen isotope hydroclimate records in water-limited SE Australia, Geochim. Cosmochim. Ac., 270, 431–448, https://doi.org/10.1016/j.gca.2019.12.007, 2020.

McDonough, L. K., Treble, P. C., Baker, A., Borsato, A., Frisia, S., Nagra, G., Coleborn, K., Gagan, M. K., Zhao, J., and Paterson, D.: Past fires and post-fire impacts reconstructed from a southwest Australian stalagmite, Geochim. Cosmochim. Ac., 325, 258–277, https://doi.org/10.1016/j.gca.2022.03.020, 2022.

Meckler, A. N., Clarkson, M. O., Cobb, K. M., Sodemann, H., and Adkins, J. F.: Interglacial Hydroclimate in the Tropical West Pacific Through the Late Pleistocene, Science, 336, 1301–1304, https://doi.org/10.1126/science.1218340, 2012.

Medina-Elizalde, M., Perritano, S., DeCesare, M., Polanco-Martinez, J., Lases-Hernandez, F., Serrato-Marks, G., and McGee, D.: Southeastern United States Hydroclimate During Holocene Abrupt Climate Events: Evidence From New Stalagmite Isotopic Records From Alabama, Paleoceanogr. Paleocl., 37, e2021PA004346, https://doi.org/10.1029/2021PA004346, 2022.

Moreno, A., Stoll, H., Jiménez-Sánchez, M., Cacho, I., Valero-Garcés, B., Ito, E., and Edwards, R. L.: A speleothem record of glacial (25-11.6 kyr BP) rapid climatic changes from northern Iberian Peninsula, Global Planet. Change, 71, 218–231, https://doi.org/10.1016/j.gloplacha.2009.10.002, 2010.

Moseley, G. E., Spötl, C., Cheng, H., Boch, R., Min, A., and Edwards, R. L.: Termination-II interstadial/stadial climate change recorded in two stalagmites from the north European Alps, Quaternary Sci. Rev., 127, 229–239, https://doi.org/10.1016/j.quascirev.2015.07.012, 2015.

Moseley, G. E., Edwards, R. L., Lord, N. S., Spötl, C., and Cheng, H.: Speleothem record of mild and wet mid-Pleistocene climate in northeast Greenland, Sci. Adv., 7, eabe1260, https://doi.org/10.1126/sciadv.abe1260, 2021.

Nagra, G., Treble, P. C., Andersen, M. S., Fairchild, I. J., Coleborn, K., and Baker, A.: A post-wildfire response in cave dripwater chemistry, Hydrol. Earth Syst. Sci., 20, 2745–2758, https://doi.org/10.5194/hess-20-2745-2016, 2016.

Nagra, G., Treble, P. C., Andersen, M. S., Bajo, P., Hellstrom, J., and Baker, A.: Dating stalagmites in mediterranean climates using annual trace element cycles, Sci. Rep., 7, 1–12, https://doi.org/10.1038/s41598-017-00474-4, 2017.

Nehme, C., Kluge, T., Verheyden, S., Nader, F., Charalambidou, I., Weissbach, T., Gucel, S., Cheng, H., Edwards, R. L., Satterfield, L., Eiche, E., and Claeys, P.: Speleothem record from Pentadactylos cave (Cyprus): new insights into climatic variations during MIS 6 and MIS 5 in the Eastern Mediterranean, Quaternary Sci. Rev., 250, 106663, https://doi.org/10.1016/j.quascirev.2020.106663, 2020.

Nehme, C., Verheyden, S., Kluge, T., Nader, F. H., Edwards, R. L., Cheng, H., Eiche, E., and Claeys, P.: Climate variability in the northern Levant from the highly resolved Qadisha record (Lebanon) during the Holocene optimum, Quaternary Res., 1–15, https://doi.org/10.1017/qua.2023.24, 2023.

Novello, V. F., Vuille, M., Cruz, F. W., Stríkis, N. M., Paula, M. S. D., Edwards, R. L., Cheng, H., Karmann, I., Jaqueto, P. F., Trindade, R. I. F., Hartmann, G. A., and Moquet, J. S.: Centennial-scale solar forcing of the South American Monsoon System recorded in stalagmites, Sci. Rep., 6, 24762, https://doi.org/10.1038/srep24762, 2016.

Novello, V. F., Cruz, F. W., Vuille, M., Stríkis, N. M., Edwards, R. L., Cheng, H., Emerick, S., de Paula, M. S., Li, X., Barreto, E. de S., Karmann, I., and Santos, R. V.: A high-resolution history of the South American Monsoon from Last Glacial Maximum to the Holocene, Sci. Rep., 7, 44267, https://doi.org/10.1038/srep44267, 2017.

Novello, V. F., Cruz, F. W., Moquet, J. S., Vuille, M., de Paula, M. S., Nunes, D., Edwards, R. L., Cheng, H., Karmann, I., Utida, G., Stríkis, N. M., and Campos, J. L. P. S.: Two Millennia of South Atlantic Convergence Zone Variability Reconstructed From Isotopic Proxies, Geophys. Res. Lett., 45, 5045–5051, https://doi.org/10.1029/2017GL076838, 2018.

Novello, V. F., Cruz, F. W., McGlue, M. M., Wong, C. I., Ward, B. M., Vuille, M., Santos, R. A., Jaqueto, P., Pessenda, L. C. R., Atorre, T., Ribeiro, L. M. A. L., Karmann, I., Barreto, E. S., Cheng, H., Edwards, R. L., Paula, M. S., and Scholz, D.: Vegetation and environmental changes in tropical South America from the last glacial to the Holocene documented by multiple cave sediment proxies, Earth Planet. Sc. Lett., 524, 115717, https://doi.org/10.1016/j.epsl.2019.115717, 2019.

Novello, V. F., William da Cruz, F., Vuille, M., Pereira Silveira Campos, J. L., Stríkis, N. M., Apaéstegui, J., Moquet, J. S., Azevedo, V., Ampuero, A., Utida, G., Wang, X., Paula-Santos, G. M., Jaqueto, P., Ruiz Pessenda, L. C., Breecker, D. O., and Karmann, I.: Investigating δ13C values in stalagmites from tropical South America for the last two millennia, Quaternary Sci. Rev., 255, 106822, https://doi.org/10.1016/j.quascirev.2021.106822, 2021.

Oster, J. L., Warken, S. F., Sekhon, N., Arienzo, M. M., and Lachniet, M.: Speleothem Paleoclimatology for the Caribbean, Central America, and North America, Quaternary, 2, 5, https://doi.org/10.3390/quat2010005, 2019.

Oster, J. L., Weisman, I. E., and Sharp, W. D.: Multiproxy stalagmite records from northern California reveal dynamic patterns of regional hydroclimate over the last glacial cycle, Quaternary Sci. Rev., 241, 106411, https://doi.org/10.1016/j.quascirev.2020.106411, 2020.

Owen, R. A., Day, C. C., Hu, C., Liu, Y., Pointing, M. D., Blättler, C. L., and Henderson, G. M.: Calcium isotopes in caves as a proxy for aridity: Modern calibration and application to the 8.2 kyr event, Earth Planet. Sc. Lett., 443, 129–138, https://doi.org/10.1016/j.epsl.2016.03.027, 2016.

Parker, S. E. and Harrison, S. P.: The timing, duration and magnitude of the 8.2 ka event in global speleothem records, Sci. Rep., 12, 10542, https://doi.org/10.1038/s41598-022-14684-y, 2022.

Parker, S. E., Harrison, S. P., and Braconnot, P.: Speleothem records of monsoon interannual-interdecadal variability through the Holocene, Environ. Res. Commun., 3, 121002, https://doi.org/10.1088/2515-7620/ac3eaa, 2021a.

Parker, S. E., Harrison, S. P., Comas-Bru, L., Kaushal, N., LeGrande, A. N., and Werner, M.: A data–model approach to interpreting speleothem oxygen isotope records from monsoon regions, Clim. Past, 17, 1119–1138, https://doi.org/10.5194/cp-17-1119-2021, 2021b.

Pérez-Mejías, C., Moreno, A., Sancho, C., Martín-García, R., Spötl, C., Cacho, I., Cheng, H., and Edwards, R. L.: Orbital-to-millennial scale climate variability during Marine Isotope Stages 5 to 3 in northeast Iberia, Quaternary Sci. Rev., 224, 105946, https://doi.org/10.1016/j.quascirev.2019.105946, 2019.

Pérez-Mejías, C., Moreno, A., Bernal-Wormull, J., Cacho, I., Osácar, M. C., Edwards, R. L., and Cheng, H.: Oldest Dryas hydroclimate reorganization in the eastern Iberian Peninsula after the iceberg discharges of Heinrich Event 1, Quaternary Res., 101, 67–83, https://doi.org/10.1017/qua.2020.112, 2021.

Priestley, S. C., Treble, P. C., Griffiths, A. D., Baker, A., Abram, N. J., and Meredith, K. T.: Caves demonstrate decrease in rainfall recharge of southwest Australian groundwater is unprecedented for the last 800 years, Commun. Earth Environ., 4, 1–12, https://doi.org/10.1038/s43247-023-00858-7, 2023.

Rehfeld, K. and Bühler, J.: Age-depth model ensembles for SISAL v3 speleothem records, Zenodo [data set], https://doi.org/10.5281/zenodo.10726619, 2024.

Riechelmann, D. F. C., Fohlmeister, J., Kluge, T., Jochum, K. P., Richter, D. K., Deininger, M., Friedrich, R., Frank, N., and Scholz, D.: Evaluating the potential of tree-ring methodology for cross-dating of three annually laminated stalagmites from Zoolithencave (SE Germany), Quaternary Geochronology, 52, 37–50, https://doi.org/10.1016/j.quageo.2019.04.001, 2019.

Riechelmann, D. F. C., Riechelmann, S., Wassenburg, J. A., Fohlmeister, J., Schöne, B. R., Jochum, K. P., Richter, D. K., and Scholz, D.: High-Resolution Proxy Records From Two Simultaneously Grown Stalagmites From Zoolithencave (Southeastern Germany) and their Potential for Palaeoclimate Reconstruction, Geochem. Geophys. Geosyst., 21, e2019GC008755, https://doi.org/10.1029/2019GC008755, 2020.

Roberts, M. S., Smart, P. L., and Baker, A.: Annual trace element variations in a Holocene speleothem, Earth Planet. Sc. Lett., 154, 237–246, https://doi.org/10.1016/s0012-821x(97)00116-7, 1998.

Roesch, C. and Rehfeld, K.: SISAL.AM, GitHub [code], https://github.com/paleovar/SISAL.AM (last access: 8 March 2024), 2020.

Ros, A. and Llamusí, J. L.: Reconstrucción y génesis del karst de Cueva Victoria, Mastia: Revista del Museo Arqueológico Municipal de Cartagena, 111–125, 2012.

Rowe, P. J., Wickens, L. B., Sahy, D., Marca, A. D., Peckover, E., Noble, S., Özkul, M., Baykara, M. O., Millar, I. L., and Andrews, J. E.: Multi-proxy speleothem record of climate instability during the early last interglacial in southern Turkey, Palaeogeogr. Palaeocl., 538, 109422, https://doi.org/10.1016/j.palaeo.2019.109422, 2020.

Rutlidge, H., Baker, A., Marjo, C. E., Andersen, M. S., Graham, P. W., Cuthbert, M. O., Rau, G. C., Roshan, H., Markowska, M., Mariethoz, G., and Jex, C. N.: Dripwater organic matter and trace element geochemistry in a semi-arid karst environment: Implications for speleothem paleoclimatology, Geochim. Cosmochim. Ac., 135, 217–230, https://doi.org/10.1016/j.gca.2014.03.036, 2014.

Scroxton, N., Walczak, M., Markowska, M., Zhao, J., and Fallon, S.: Historical droughts in Southeast Australia recorded in a New South Wales stalagmite, The Holocene, 31, 607–617, https://doi.org/10.1177/0959683620981717, 2021.

Serrato Marks, G., Medina-Elizalde, M., Burns, S., Weldeab, S., Lases-Hernandez, F., Cazares, G., and McGee, D.: Evidence for Decreased Precipitation Variability in the Yucatán Peninsula During the Mid-Holocene, Paleoceanogr. Paleocl., 36, e2021PA004219, https://doi.org/10.1029/2021PA004219, 2021.

Sha, L., Ait Brahim, Y., Wassenburg, J. A., Yin, J., Peros, M., Cruz, F. W., Cai, Y., Li, H., Du, W., Zhang, H., Edwards, R. L., and Cheng, H.: How Far North Did the African Monsoon Fringe Expand During the African Humid Period? Insights From Southwest Moroccan Speleothems, Geophys. Res. Lett., 46, 14093–14102, https://doi.org/10.1029/2019GL084879, 2019.

Sha, L., Brahim, Y. A., Wassenburg, J. A., Yin, J., Lu, J., Cruz, F. W., Cai, Y., Edwards, R. L., and Cheng, H.: The "Hockey Stick" Imprint in Northwest African Speleothems, Geophys. Res. Lett., 48, e2021GL094232, https://doi.org/10.1029/2021GL094232, 2021.

Sinha, A., Kathayat, G., Cheng, H., Breitenbach, S. F. M., Berkelhammer, M., Mudelsee, M., Biswas, J., and Edwards, R. L.: Trends and oscillations in the Indian summer monsoon rainfall over the last two millennia, Nat. Commun., 6, 6309, https://doi.org/10.1038/ncomms7309, 2015.

Sinha, A., Kathayat, G., Weiss, H., Li, H., Cheng, H., Reuter, J., Schneider, A. W., Berkelhammer, M., Adalı, S. F., Stott, L. D., and Edwards, R. L.: Role of climate in the rise and fall of the Neo-Assyrian Empire, Sci. Adv., 5, eaax6656, https://doi.org/10.1126/sciadv.aax6656, 2019.

Skiba, V.: SISALv3 trace element downsampling code, Zenodo [code], https://doi.org/10.5281/zenodo.8234066, 2023.

Skiba, V. and Fohlmeister, J.: Contemporaneously growing speleothems and their value to decipher in-cave processes – A modelling approach, Geochim. Cosmochim. Ac., 348, 381–396, https://doi.org/10.1016/j.gca.2023.03.016, 2023.

Skiba, V., Jouvet, G., Marwan, N., Spötl, C., and Fohlmeister, J.: Speleothem growth and stable carbon isotopes as proxies of the presence and thermodynamical state of glaciers compared to modelled glacier evolution in the Alps, Quaternary Sci. Rev., 322, 108403, https://doi.org/10.1016/j.quascirev.2023.108403, 2023.

Stoll, H., Mendez-Vicente, A., Gonzalez-Lemos, S., Moreno, A., Cacho, I., Cheng, H., and Edwards, R. L.: Interpretation of orbital scale variability in mid-latitude speleothem d18O: Significance of growth rate controlled kinetic frac-

tionation effects, Quaternary Sci. Rev., 127, 215–228, https://doi.org/10.1016/j.quascirev.2015.08.025, 2015.

Stoll, H. M., Cacho, I., Gasson, E., Sliwinski, J., Kost, O., Moreno, A., Iglesias, M., Torner, J., Perez-Mejias, C., Haghipour, N., Cheng, H., and Edwards, R. L.: Rapid northern hemisphere ice sheet melting during the penultimate deglaciation, Nat. Commun., 13, 3819, https://doi.org/10.1038/s41467-022-31619-3, 2022.

Stoll, H. M., Day, C., Lechleitner, F., Kost, O., Endres, L., Sliwinski, J., Pérez-Mejías, C., Cheng, H., and Scholz, D.: Distinguishing the combined vegetation and soil component of δ^{13}C variation in speleothem records from subsequent degassing and prior calcite precipitation effects, Clim. Past, 19, 2423–2444, https://doi.org/10.5194/cp-19-2423-2023, 2023.

Stríkis, N. M., Cruz, F. W., Barreto, E. A. S., Naughton, F., Vuille, M., Cheng, H., Voelker, A. H. L., Zhang, H., Karmann, I., Edwards, R. L., Auler, A. S., Santos, R. V., and Sales, H. R.: South American monsoon response to iceberg discharge in the North Atlantic, P. Natl. Acad. Sci. USA, 115, 3788–3793, https://doi.org/10.1073/pnas.1717784115, 2018.

Surić, M., Columbu, A., Lončarić, R., Bajo, P., Bočić, N., Lončar, N., Drysdale, R. N., and Hellstrom, J. C.: Holocene hydroclimate changes in continental Croatia recorded in speleothem δ^{13}C and δ^{18}O from Nova Grgosova Cave, The Holocene, 31, 1401–1416, https://doi.org/10.1177/09596836211019120, 2021a.

Surić, M., Bajo, P., Lončarić, R., Lončar, N., Drysdale, R. N., Hellstrom, J. C., and Hua, Q.: Speleothem Records of the Hydroclimate Variability throughout the Last Glacial Cycle from Manita peć Cave (Velebit Mountain, Croatia), Geosciences, 11, 347, https://doi.org/10.3390/geosciences11080347, 2021b.

Tadros, C. V., Treble, P. C., Baker, A., Fairchild, I., Hankin, S., Roach, R., Markowska, M., and McDonald, J.: ENSO–cave drip water hydrochemical relationship: a 7-year dataset from south-eastern Australia, Hydrol. Earth Syst. Sci., 20, 4625–4640, https://doi.org/10.5194/hess-20-4625-2016, 2016.

Tadros, C. V., Markowska, M., Treble, P. C., Baker, A., Frisia, S., Adler, L., and Drysdale, R. N.: Recharge variability in Australia's southeast alpine region derived from cave monitoring and modern stalagmite δ18O records, Quaternary Sci. Rev., 295, 107742, https://doi.org/10.1016/j.quascirev.2022.107742, 2022.

Tan, L., Li, Y., Wang, X., Cai, Y., Lin, F., Cheng, H., Ma, L., Sinha, A., and Edwards, R. L.: Holocene Monsoon Change and Abrupt Events on the Western Chinese Loess Plateau as Revealed by Accurately Dated Stalagmites, Geophys. Res. Lett., 47, e2020GL090273, https://doi.org/10.1029/2020GL090273, 2020a.

Tan, L., Liu, W., Wang, T., Cheng, P., Zang, J., Wang, X., Ma, L., Li, D., Lan, J., Edwards, R. L., Cheng, H., Xu, H., Ai, L., Gao, Y., and Cai, Y.: A multiple-proxy stalagmite record reveals historical deforestation in central Shandong, northern China, Sci. China Earth Sci., 63, 1622–1632, https://doi.org/10.1007/s11430-019-9649-1, 2020b.

Tan, L., Dong, G., An, Z., Lawrence Edwards, R., Li, H., Li, D., Spengler, R., Cai, Y., Cheng, H., Lan, J., Orozbaev, R., Liu, R., Chen, J., Xu, H., and Chen, F.: Megadrought and cultural exchange along the proto-silk road, Sci. Bull., 66, 603–611, https://doi.org/10.1016/j.scib.2020.10.011, 2021.

Torner, J., Cacho, I., Moreno, A., Sierro, F. J., Martrat, B., Rodriguez-Lazaro, J., Frigola, J., Arnau, P., Belmonte, Á., Hellstrom, J., Cheng, H., Edwards, R. L., and Stoll, H.: Ocean-atmosphere interconnections from the last interglacial to the early glacial: An integration of marine and cave records in the Iberian region, Quaternary Sci. Rev., 226, 106037, https://doi.org/10.1016/j.quascirev.2019.106037, 2019.

Treble, P., Shelley, J. M. G., and Chappell, J.: Comparison of high resolution sub-annual records of trace elements in a modern (1911-1992) speleothem with instrumental climate data from southwest Australia, Earth Planet. Sc. Lett., 216, 141–153, https://doi.org/10.1016/S0012-821X(03)00504-1, 2003.

Treble, P. C., Baker, A., Abram, N. J., Hellstrom, J. C., Crawford, J., Gagan, M. K., Borsato, A., Griffiths, A. D., Bajo, P., Markowska, M., Priestley, S. C., Hankin, S., and Paterson, D.: Ubiquitous karst hydrological control on speleothem oxygen isotope variability in a global study, Commun. Earth Environ., 3, 29, https://doi.org/10.1038/s43247-022-00347-3, 2022.

Tremaine, D. M. and Froelich, P. N.: Speleothem trace element signatures: A hydrologic geochemical study of modern cave dripwaters and farmed calcite, Geochim. Cosmochim. Ac., 121, 522–545, https://doi.org/10.1016/j.gca.2013.07.026, 2013.

Ünal-İmer, E., Shulmeister, J., Zhao, J.-X., Tonguç Uysal, I., Feng, Y.-X., Duc Nguyen, A., and Yüce, G.: An 80 kyr-long continuous speleothem record from Dim Cave, SW Turkey with paleoclimatic implications for the Eastern Mediterranean, Sci. Rep., 5, 13560, https://doi.org/10.1038/srep13560, 2015.

Ünal-İmer, E., Shulmeister, J., Zhao, J.-X., Uysal, I. T., and Feng, Y.-X.: High-resolution trace element and stable/radiogenic isotope profiles of late Pleistocene to Holocene speleothems from Dim Cave, SW Turkey, Palaeogeogr. Palaeocl., 452, 68–79, https://doi.org/10.1016/j.palaeo.2016.04.015, 2016.

Utida, G., Cruz, F. W., Santos, R. V., Sawakuchi, A. O., Wang, H., Pessenda, L. C. R., Novello, V. F., Vuille, M., Strauss, A. M., Borella, A. C., Stríkis, N. M., Guedes, C. C. F., Dias De Andrade, F. R., Zhang, H., Cheng, H., and Edwards, R. L.: Climate changes in Northeastern Brazil from deglacial to Meghalayan periods and related environmental impacts, Quaternary Sci. Rev., 250, 106655, https://doi.org/10.1016/j.quascirev.2020.106655, 2020.

Verheyden, S., Keppens, E., Fairchild, I. J., McDermott, F., and Weis, D.: Mg, Sr and Sr isotope geochemistry of a Belgian Holocene speleothem: Implications for paleoclimate reconstructions, Chem. Geol., 169, 131–144, https://doi.org/10.1016/S0009-2541(00)00299-0, 2000.

Wainer, K., Genty, D., Blamart, D., Daëron, M., Bar-Matthews, M., Vonhof, H., Dublyansky, Y., Pons-Branchu, E., Thomas, L., van Calsteren, P., Quinif, Y., and Caillon, N.: Speleothem record of the last 180 ka in Villars cave (SW France): Investigation of a large δ^{18}O shift between MIS6 and MIS5, Quaternary Sci. Rev., 30, 130–146, https://doi.org/10.1016/j.quascirev.2010.07.004, 2011.

Waltgenbach, S., Scholz, D., Spötl, C., Riechelmann, D. F. C., Jochum, K. P., Fohlmeister, J., and Schröder-Ritzrau, A.: Climate and structure of the 8.2 ka event reconstructed from three speleothems from Germany, Global Planet. Change, 193, 103266, https://doi.org/10.1016/j.gloplacha.2020.103266, 2020.

Waltgenbach, S., Riechelmann, D. F. C., Spötl, C., Jochum, K. P., Fohlmeister, J., Schröder-Ritzrau, A., and Scholz, D.: Climate Variability in Central Europe during the Last 2500 Years Reconstructed from Four High-Resolution

Multi-Proxy Speleothem Records, Geosciences, 11, 166, https://doi.org/10.3390/geosciences11040166, 2021.

Wang, Y. J., Cheng, H., Edwards, R. L., An, Z. S., Wu, J. Y., Shen, C. C., and Dorale, J. A.: A high-resolution absolute-dated late Pleistocene Monsoon record from Hulu Cave, China., Science (New York, N.Y.), 294, 2345–2348, https://doi.org/10.1126/science.1064618, 2001.

Ward, B. M., Wong, C. I., Novello, V. F., McGee, D., Santos, R. V., Silva, L. C. R., Cruz, F. W., Wang, X., Edwards, R. L., and Cheng, H.: Reconstruction of Holocene coupling between the South American Monsoon System and local moisture variability from speleothem δ18O and 87Sr/86Sr records, Quaternary Sci. Rev., 210, 51–63, https://doi.org/10.1016/j.quascirev.2019.02.019, 2019.

Warken, S. F., Fohlmeister, J., Schröder-Ritzrau, A., Constantin, S., Spötl, C., Gerdes, A., Esper, J., Frank, N., Arps, J., Terente, M., Riechelmann, D. F. C., Mangini, A., and Scholz, D.: Reconstruction of late Holocene autumn/winter precipitation variability in SW Romania from a high-resolution speleothem trace element record, Earth Planet. Sc. Lett., 499, 122–133, https://doi.org/10.1016/j.epsl.2018.07.027, 2018.

Warken, S. F., Vieten, R., Winter, A., Spötl, C., Miller, T. E., Jochum, K. P., Schröder-Ritzrau, A., Mangini, A., and Scholz, D.: Persistent Link Between Caribbean Precipitation and Atlantic Ocean Circulation During the Last Glacial Revealed by a Speleothem Record From Puerto Rico, Paleoceanogr. Paleocl., 35, e2020PA003944, https://doi.org/10.1029/2020PA003944, 2020.

Warken, S. F., Schorndorf, N., Stinnesbeck, W., Hennhoefer, D., Stinnesbeck, S. R., Förstel, J., Steidle, S. D., Avilés Olguin, J., and Frank, N.: Solar forcing of early Holocene droughts on the Yucatán peninsula, Sci. Rep., 11, 13885, https://doi.org/10.1038/s41598-021-93417-z, 2021.

Wassenburg, J. A., Scholz, D., Jochum, K. P., Cheng, H., Oster, J., Immenhauser, A., Richter, D. K., Häger, T., Jamieson, R. A., Baldini, J. U. L., Hoffmann, D., and Breitenbach, S. F. M.: Determination of aragonite trace element distribution coefficients from speleothem calcite–aragonite transitions, Geochim. Cosmochim. Ac., 190, 347–367, https://doi.org/10.1016/j.gca.2016.06.036, 2016.

Wassenburg, J. A., Vonhof, H. B., Cheng, H., Martínez-García, A., Ebner, P.-R., Li, X., Zhang, H., Sha, L., Tian, Y., Edwards, R. L., Fiebig, J., and Haug, G. H.: Penultimate deglaciation Asian monsoon response to North Atlantic circulation collapse, Nat. Geosci., 14, 937–941, https://doi.org/10.1038/s41561-021-00851-9, 2021.

Weber, M., Scholz, D., Schröder-Ritzrau, A., Deininger, M., Spötl, C., Lugli, F., Mertz-Kraus, R., Jochum, K. P., Fohlmeister, J., Stumpf, C. F., and Riechelmann, D. F. C.: Evidence of warm and humid interstadials in central Europe during early MIS 3 revealed by a multi-proxy speleothem record, Quaternary Sci. Rev., 200, 276–286, https://doi.org/10.1016/j.quascirev.2018.09.045, 2018.

Weber, M., Hinz, Y., Schöne, B. R., Jochum, K. P., Hoffmann, D., Spötl, C., Riechelmann, D. F. C., and Scholz, D.: Opposite Trends in Holocene Speleothem Proxy Records From Two Neighboring Caves in Germany: A Multi-Proxy Evaluation, Front. Earth Sci., 9, 642651, https://doi.org/10.3389/feart.2021.642651, 2021.

Welte, C., Fohlmeister, J., Wertnik, M., Wacker, L., Hattendorf, B., Eglinton, T. I., and Spötl, C.: Climatic variations during the Holocene inferred from radiocarbon and stable carbon isotopes in speleothems from a high-alpine cave, Clim. Past, 17, 2165–2177, https://doi.org/10.5194/cp-17-2165-2021, 2021.

Wendt, K. A., Häuselmann, A. D., Fleitmann, D., Berry, A. E., Wang, X., Auler, A. S., Cheng, H., and Edwards, R. L.: Three-phased Heinrich Stadial 4 recorded in NE Brazil stalagmites, Earth Planet. Sc. Lett., 510, 94–102, https://doi.org/10.1016/j.epsl.2018.12.025, 2019.

Wendt, K. A., Li, X., Edwards, R. L., Cheng, H., and Spötl, C.: Precise timing of MIS 7 substages from the Austrian Alps, Clim. Past, 17, 1443–1454, https://doi.org/10.5194/cp-17-1443-2021, 2021.

Wilcox, P. S., Honiat, C., Trüssel, M., Edwards, R. L., and Spötl, C.: Exceptional warmth and climate instability occurred in the European Alps during the Last Interglacial period, Commun. Earth Environ., 1, 1–6, https://doi.org/10.1038/s43247-020-00063-w, 2020.

Winter, A., Zanchettin, D., Lachniet, M., Vieten, R., Pausata, F. S. R., Ljungqvist, F. C., Cheng, H., Edwards, R. L., Miller, T., Rubinetti, S., Rubino, A., and Taricco, C.: Initiation of a stable convective hydroclimatic regime in Central America circa 9000 years BP, Nat. Commun., 11, 716, https://doi.org/10.1038/s41467-020-14490-y, 2020.

Wolf, A., Baker, J. L., Tjallingii, R., Cai, Y., Osinzev, A., Antonosyan, M., Amano, N., Johnson, K. R., Skiba, V., McCormack, J., Kwiecien, O., Chervyatsova, O. Y., Dublyansky, Y. V., Dbar, R. S., Cheng, H., and Breitenbach, S. F. M.: Western Caucasus regional hydroclimate controlled by cold-season temperature variability since the Last Glacial Maximum, Commun. Earth Environ., 5, 1–10, https://doi.org/10.1038/s43247-023-01151-3, 2024.

Wong, C. I. and Breecker, D. O.: Advancements in the use of speleothems as climate archives, Quaternary Sci. Rev., 127, 1–18, https://doi.org/10.1016/j.quascirev.2015.07.019, 2015.

Wortham, B. E., Wong, C. I., Silva, L. C. R., McGee, D., Montañez, I. P., Troy Rasbury, E., Cooper, K. M., Sharp, W. D., Glessner, J. J. G., and Santos, R. V.: Assessing response of local moisture conditions in central Brazil to variability in regional monsoon intensity using speleothem $^{87}Sr/^{86}Sr$ values, Earth Planet. Sc. Lett., 463, 310–322, https://doi.org/10.1016/j.epsl.2017.01.034, 2017.

Wright, K. T., Johnson, K. R., Bhattacharya, T., Marks, G. S., McGee, D., Elsbury, D., Peings, Y., Lacaille-Muzquiz, J., Lum, G., Beramendi-Orosco, L., and Magnusdottir, G.: Precipitation in Northeast Mexico Primarily Controlled by the Relative Warming of Atlantic SSTs, Geophys. Res. Lett., 49, e2022GL098186, https://doi.org/10.1029/2022GL098186, 2022.

Wu, Y., Li, T.-Y., Yu, T.-L., Shen, C.-C., Chen, C.-J., Zhang, J., Li, J.-Y., Wang, T., Huang, R., and Xiao, S.-Y.: Variation of the Asian summer monsoon since the last glacial-interglacial recorded in a stalagmite from southwest China, Quaternary Sci. Rev., 234, 106261, https://doi.org/10.1016/j.quascirev.2020.106261, 2020.

Yang, X., Yang, H., Wang, B., Huang, L.-J., Shen, C.-C., Edwards, R. L., and Cheng, H.: Early-Holocene monsoon instability and climatic optimum recorded

by Chinese stalagmites, The Holocene, 29, 1059–1067, https://doi.org/10.1177/0959683619831433, 2019.

Zhang, H., Ait Brahim, Y., Li, H., Zhao, J., Kathayat, G., Tian, Y., Baker, J., Wang, J., Zhang, F., Ning, Y., Edwards, R. L., and Cheng, H.: The Asian Summer Monsoon: Teleconnections and Forcing Mechanisms – A Review from Chinese Speleothem $\delta^{18}O$ Records, Quaternary, 2, 26, https://doi.org/10.3390/quat2030026, 2019.

Zhang, H., Cheng, H., Sinha, A., Spötl, C., Cai, Y., Liu, B., Kathayat, G., Li, H., Tian, Y., Li, Y., Zhao, J., Sha, L., Lu, J., Meng, B., Niu, X., Dong, X., Liang, Z., Zong, B., Ning, Y., Lan, J., and Edwards, R. L.: Collapse of the Liangzhu and other Neolithic cultures in the lower Yangtze region in response to climate change, Sci. Adv., 7, eabi9275, https://doi.org/10.1126/sciadv.abi9275, 2021a.

Zhang, H., Cheng, H., Spötl, C., Zhang, X., Cruz, F. W., Sinha, A., Auler, A. S., Stríkis, N. M., Wang, X., Kathayat, G., Li, X., Li, H., Pérez-Mejías, C., Cai, Y., Ning, Y., and Edwards, R. L.: Gradual South-North Climate Transition in the Atlantic Realm Within the Younger Dryas, Geophys. Res. Lett., 48, e2021GL092620, https://doi.org/10.1029/2021GL092620, 2021b.

Zhang, H., Zhang, X., Cai, Y., Sinha, A., Spötl, C., Baker, J., Kathayat, G., Liu, Z., Tian, Y., Lu, J., Wang, Z., Zhao, J., Jia, X., Du, W., Ning, Y., An, Z., Edwards, R. L., and Cheng, H.: A data-model comparison pinpoints Holocene spatiotemporal pattern of East Asian summer monsoon, Quaternary Sci. Rev., 261, 106911, https://doi.org/10.1016/j.quascirev.2021.106911, 2021c.

Zhao, J., Cheng, H., Yang, Y., Liu, W., Zhang, H., Li, X., Li, H., Ait-Brahim, Y., Pérez-Mejías, C., and Qu, X.: Role of the Summer Monsoon Variability in the Collapse of the Ming Dynasty: Evidences From Speleothem Records, Geophys. Res. Lett., 48, e2021GL093071, https://doi.org/10.1029/2021GL093071, 2021.

Zhao, K., Wang, Y., Edwards, R. L., Cheng, H., Kong, X., Liu, D., Shao, Q., Cui, Y., Huang, C., Ning, Y., and Yang, X.: Late Holocene monsoon precipitation changes in southern China and their linkage to Northern Hemisphere temperature, Quaternary Sci. Rev., 232, 106191, https://doi.org/10.1016/j.quascirev.2020.106191, 2020.